Chapter 5

CHAOS IN SPIN GLASSES

1. Chaos in spin glasses: the droplet model

The chaoticity of the free-energy landscape is an old problem in disordered frustrated systems [BY86, Rit94]. Recently it has attracted renewed attention due to its potential relevance in the rejuvenation of the ageing process observed experimentally in ac susceptibility measurements of spin glasses when changing the temperature [VHO92].

Within the spin-glass context the word chaos accounts for the extreme sensibility of the free-energy landscape against the introduction of infinitesimal perturbations δ such as a small change in temperature or in the random bonds, or a small applied magnetic field. The introduction of a perturbation does not take the system out of the frozen phase but changes the structure of the free-energy landscape, so that the distance in phase space between equilibrium configurations grows with perturbation strength.

As pointed out in the Introduction such a property lies at the core of the phenomenological droplet theory proposed for low-dimensional spin glasses by Bray and Moore and Fisher and Huse [BM87, FH88a]. Within this picture, the relative spin orientations are increasingly sensitive with increasing distance to an external perturbation $\delta \ll 1$, so that the equilibrium state changes completely beyond a certain length scale $L_c^*(\delta)$. Consider the ground state of a given sample. The energetic cost of overturning a droplet is JL^θ where J is a measure of the bond strength and $\theta < (d-1)/2$ [1]. The spins lying at the surface are assumed to be very sensible to perturbations, so that when $\delta \neq 0$ these can randomly change orientations. Since a droplet has a fractal surface $d-1 < d_s < d$, the energy of the new ground state is increased by a factor $\delta\,\sigma\,L^{d_s/2}$, σ being the entropy stiffness constant. Thus, as long as $d_s/2 > \theta$, the droplet might be energetically favoured

[1] We note that J is the zero temperature equivalent of the stiffness constant $\Upsilon(T)$ introduced in the Introduction (Sec. 2.3).

at length scales larger than,

$$L_c(\delta) = \left(\frac{J}{\delta\,\sigma}\right)^{1/\zeta} \qquad \zeta = \frac{d_s}{2} - \theta \tag{5.1}$$

where ζ is the so called chaos exponent. This crossover length scale diverges when δ is set to zero but remains finite for any non-vanishing perturbation so that two copies of the system are completely uncorrelated when taking the limit $L \to \infty$. Here, like in phase transitions, the order in which limits are taken is very important: one must take the infinite-volume limit keeping δ fixed and finally take the limit $\delta \to 0$ to obtain meaningful results.

The existence of chaos under magnetic and bond strength perturbations has been thoroughly studied and is well established for mean-field as well as short-ranged spin glass systems [BM87, Rit94, AFR95, RSB$^+$96a, NN97]. However, the most intriguing case is to elucidate whether there is *chaos with temperature* because this is not understood at a theoretical level and has been the subject of recent experimental investigation. Explicit results have only been only obtained for some Migdal-Kadanoff type real space renormalisation-group (MKRG) studies [BB87, NNH93].

Early studies of mean-field models assumed that there was chaos with temperature even though with a slightly different meaning. Such an assumption derived from the knowledge that in the SK model there are many metastable states which have a free-energy difference of $\mathcal{O}(1)$ [MPV87]. A change in temperature results in a reshuffling of the statistical weights of these states, the equilibrium state being a different one. However, the study of saddle-point solutions reveals that there can exist global solutions with and without correlations between the equilibrium states at different temperatures [Som85, Kon89, KV93, FNN95]. The most recent study made by Crisanti and Rizzo [CR02b] reveals that there is chaos in the SK model but that this effect is very small and very difficult to observe numerically [Rit94, AFR95, NN97, HK97, BM00, MPP01, BM02]. However, this is not the case in spherical p-spin models where there is a solution in which the overlap between two systems at different temperatures remains finite for any $\delta T \neq 0$ [Riz01, Riz02].

Certainly, chaos is linked with the existence of low cost system-size excitations which completely change the equilibrium state. Thus the study of the sensitiveness of the actual ground-state configuration to a perturbation is another way to understand the role of these excitations. Besides it is very interesting to analyse the dynamical counterpart of these excitations to try to understand what leads to strong *rejuvenation* and absence of cooling rate effects in the ageing process at low temperatures (see Sec. 1.3).

It is out of question that a system that displays chaos in temperature would exhibit such effects. Still, it is interesting to study the opposite situation: is it really necessary to have static chaos in order to observe *chaotic* effects? The underlying mechanism leading to strong rejuvenation effects is the large response to a change in temperature. This can be achieved in the absence of true chaos if the dynamics at different temperatures take place at different length scales. The restart of the ageing process when lowering the temperature

would be due to the relaxation of smaller length scales that have fallen out of equilibrium. This is the alternative explanation proposed by hierarchical models [VHO$^+$96].

However, it is still not clear whether true chaos exists or not in real systems. Recent experiments have been interpreted in terms of overlap lengths [JYN02a], but numerical simulations of the EA model in 3d have not been able to find chaos [PRTR01b, PRTR01a] but only rejuvenation effects associated to scale freezing in the case of 4d [BB02]. As a matter of fact, temperature chaos is so difficult to observe in the 3d EA model because the lattice sizes which can be thermalised are roughly of the order of the crossover length [ABM02]. This puts forward the idea that if short-ranged spin glasses were chaotic, the existence of such large crossover length scales would make it difficult to identify static chaos with the *chaotic* phenomena observed experimentally, as the typical length scales grown in experiments are too small. However, we cannot rule out the possibility that at small length scales there arise weak perturbation regime effects due to the existence of true chaos at large length scales.

In this chapter we propose a comprehensive study of what type of excitations lead to temperature chaos and what is their relevance in rejuvenation. We investigate three different models: the directed polymer in random media (DPRM) [HHH93], the random-energy (exponential) model (REEM) [Der81] and the Sinai model [Sin81]. The interest of the DPRM relies on its simplicity that allows us analyse what is the effect of perturbations through scaling arguments. In turn, we gain the knowledge of how this chaoticity in real space is seen in replica space mapping the onset of chaos with the onset of replica symmetry breaking. For this situation to take place it is important that the stable (replica) solution of the saddle point equations is marginally stable.

The REM and the Sinai models are two well known random potential models. In the former we will see that the existence of a delocalisation transition leads to chaotic effects which can yield rejuvenation and memory effects very similar to those found experimentally [SN00, Kaw01]. The Sinai model is the simplest model where the energy landscape is *explicitly hierarchical*. In high dimensions, this problem is equivalent to a mean-field spin-glass with a continuous replica symmetry breaking solution [MP91]. In one dimension, however, there is no phase transition: the long-time, large-scale behaviour of the system is ruled by the zero-temperature fixed point, where the deepest minimum determines low-T behaviour. There is no true chaos in this model, but still the are crossover effects leading to embryonic rejuvenation and memory effects.

1.1 Correlation functions; a definition of chaos in replica space

To elucidate the chaotic properties of a system one needs to study the correlations between two identical copies of the same system, also called *real replicas* A and B. The bare Hamiltonian describing each replica is $\mathcal{H}_0^{\rm X}, \ \ {\rm X} = {\rm A},\ {\rm B}$. Now, if we introduce a perturbation δ to replica B the global Hamiltonian reads,

$$\mathcal{H} = \mathcal{H}_0^{\rm A} + \mathcal{H}_0^{\rm B} + \mathcal{H}_1(\delta) \ , \tag{5.2}$$

where $\mathcal{H}_1(\delta)$ stands for the perturbation term [2].

In spin systems the usual measure of the distance between the configurations of the unperturbed replica A $\{\sigma^{\rm A}\}$ and of the perturbed one B $\{\sigma^{\rm B}\}$ is the overlap between both,

$$q_{\rm AB} = \frac{1}{V}\sum_{i=1,V} \langle \sigma_i^{\rm A}\ \sigma_i^{\rm B}\rangle_{\mathcal{H}} \tag{5.3}$$

where V is the number of spins and the thermal average is taken with respect to the global Hamiltonian (5.2). The first analytical approaches tried to see whether solutions with $q_{\rm AB} \neq 0$ where stable by means of perturbation methods. Following this direction the distribution of the cross-overlap has been studied. In this situation the system is non chaotic if the $P(q_{\rm AB})$ is a non-trivial function of $q_{\rm AB}$ [BM00, BM02]. It is also useful to define the following adimensional parameters r and a [Rit94],

$$r(\delta) = \frac{\overline{\langle \sigma_i^{\rm A}\ \sigma_i^{\rm B}\rangle_{\mathcal{H}}}}{\sqrt{\overline{\langle \sigma_i^{\rm A}\ \sigma_i^{\rm A}\rangle}_{\mathcal{H}_I^{\rm A}}\ \overline{\langle \sigma_i^{\rm B}\ \sigma_i^{\rm B}\rangle}_{\mathcal{H}_I^{\rm B}}}}\,; \qquad a(\delta) = \frac{\overline{\langle \sigma_i^{\rm A}\ \sigma_i^{\rm B}\rangle}_{\mathcal{H}}}{\overline{\langle \sigma_i^{\rm A}\ \sigma_i^{\rm A}\rangle}_{\mathcal{H}_I^{\rm A}}} \tag{5.4}$$

which fulfil the requirement that if the equilibrium configurations are the same (i.e. when $\delta = 0$) r and a are equal to 1. Whereas if the system is chaotic these parameters are smaller than 1 in the thermodynamic limit [3].

Here, we will follow a different approach. From the point of view of configurational space one can address the problem by probing directly the free-energy landscape. In a random system, the free-energy is also a random variable with a certain distribution law whose average is $\overline{F} = -T\overline{\ln \mathcal{Z}}$. Thus the value of the free-energy for a certain realisation of the couplings has a deviation from the mean: $\Phi = F - \overline{F}$. To study the change in the free-energy landscape under a perturbation, we need to analyse if the free-energy fluctuations of systems A and B are correlated when $\delta \neq 0$. We can construct the following correlation function [FH91b],

$$C_F(L,\delta) = \frac{\overline{\Phi_{\rm A}(L)\Phi_{\rm B}(L)}}{\sqrt{\overline{\Phi_{\rm A}^2(L)}}\,;\,\sqrt{\overline{\Phi_{\rm B}^2(L)}}}\,; \qquad \Phi_{\rm A,B} = F_{\rm A,B} - \overline{F_{\rm A,B}} \tag{5.5}$$

If the correlation function vanishes at large length scales

$$\lim_{\delta\to 0}\ \lim_{L\to\infty}\ C_F(L,\delta) \to 0 \tag{5.6}$$

this implies that the free-energy landscapes of A and B decorrelate completely. If this statistical decoupling takes place in the thermodynamic limit even when the perturbation is arbitrarily weak, $\delta \ll 1$, we say that there is *chaos*. The measure of chaos was

[2] Note that here the global Hamiltonian corresponding to B is $\mathcal{H}^{\rm B} = \mathcal{H}_0^{\rm B} + \mathcal{H}_1(\delta)$.

[3] We have to point out that one has to be careful when investigating these parameters close to the critical temperature where parameter a might vanish even in the absence of true chaos [Rit94].

originally introduced in terms of correlation functions by Bray and Moore [BM87], who put forward that in a chaotic system the correlations should vanish exponentially as $\sim \exp\left(-L/L_c(\delta)\right)$ under the addition of an external perturbation δ. This is the case of spin glasses when a magnetic field is introduced or the random bonds are perturbed. However, here we assume that there is chaos when correlations vanish in the thermodynamical limit, even if the decay is not exponential. In this situation, one can still define an overlap length scale signalling the crossover between a weak perturbation regime with a power-law decay, to a strong perturbation regime with a faster decay that might be stretched or barely exponential [SY02].

Our main concern is to analyse the temperature chaos problem. Already a very simple argument can help us to make some insight in what are the relevant ingredients leading to a significant change in the free-energy landscape when the temperature is shifted. If we consider a system with N different states of energies ϵ_i with a given statistics, the partition function at temperature $T = \beta^{-1}$ reads $\mathcal{Z} = \sum_i \exp\left(-\beta\epsilon_i\right)$. Consider two systems A and B at different temperatures very close to T such that $T_{\rm A} = T(1-\delta)$ and $T_{\rm B} = T(1+\delta)$, with $\delta \ll 1$. Using the thermodynamic relations for the entropy $S = -\frac{\partial F}{\partial T}$ and the heat capacity $\mathrm{C} = T\frac{\partial S}{\partial T}$ we obtain that the free-energy at $T_{\rm A}$ reads,

$$F_{\rm A} = F(T) + \ \delta\ TS(T) + \ \frac{1}{2}\,\delta^2\ T\ \mathrm{C}(T) + \mathcal{O}(\delta^3) \tag{5.7}$$

Hence, up to order δ^2 the difference of free-energy between both systems for a given realisation of the disorder has an entropic origin [4],

$$\delta\ F \equiv F_{\rm B} - F_{\rm A} = 2\delta TS(T) + \mathcal{O}(\delta^3) = (T_2 - T_1)S(T) + \mathcal{O}(\delta^3) \tag{5.8}$$

This result can be used to simplify the expression for C_F in (5.5). We observe that the numerator and denominator in C_F can be reexpressed as follows,

$$\Phi_{\rm B} = \Phi_{\rm A} + \phi\,; \qquad \phi = \delta F - \overline{\delta F}$$

$$\text{numerator} = \overline{(\Phi_{\rm A})^2} + \overline{\Phi_{\rm A}\phi} \tag{5.9}$$

$$\text{denominator} = \sqrt{\overline{(\Phi_{\rm A})^2}}\sqrt{\overline{(\Phi_{\rm A}+\phi)^2}}\ . \tag{5.10}$$

As long as δT is small, $\phi \ll \Phi_{\rm A}$, thereby we can expand numerator and denominator to obtain the following result for C_F,

$$C_F \approx 1 - \frac{1}{2}\frac{\overline{\phi^2}}{\overline{\Phi_T^2}} = 1 - \frac{(2\delta)^2\,T^2}{2}\frac{\overline{\left(\Delta S(T)\right)^2}}{\overline{\Phi_T^2}} = 1 - \kappa_F\delta^2\,; \qquad \Delta S = S = \overline{S} \tag{5.11}$$

where we have used that $\Phi_{\rm A} = \Phi_T + \mathcal{O}(\delta^2)$. In the last equality we have defined the susceptibility κ_F which measures the response of the system to temperature changes:

[4] Note that in (5.8) there is no term $\mathcal{O}(\delta^2)$ because we consider $T_{\rm A/B} = T(1 \pm \delta)$. Considering different $T_{\rm A/B}$ would imply a non zero term of order δ^2, but this would not alter the result because the leading term is linear in δ.

if κ_F diverges in the limit $L \to \infty$ the system is chaotic. In the scaling picture of spin glasses when we consider temperature changes it is assumed that $\Phi = \Upsilon(T)\, L^{\theta}$ and $\Delta S = \sigma(T)\, L^{d_s/2}$ where we have introduced the generalised stiffness constants associated to free-energy and entropy $\Upsilon(T)$ and $\sigma(T)$. Hence we expect that the following functional dependence for the correlation,

$$1 - C_F \sim (L/L_c)^{2\zeta} \tag{5.12}$$

where ζ has been defined in (5.1) and L_c is generalised to $L_c = \left(\frac{\Upsilon}{\sigma\, \delta T}\right)$. This same relation had already been derived by Bray and Moore in [BM87] for any kind of perturbation in the limit $\delta \ll 1$. On general grounds we expect that if the system is chaotic C_F is a scaling function $f\,(L/L_c)$ with the appropriate overlap length.

The importance of the result in (5.11) is that a system is chaotic if entropy fluctuations grow faster with system size than free-energy fluctuations. This fact was already noted by Banavar and Bray in [BB87] in MK spin glasses, and means that the equilibrium state changes with temperature if there exist excited states with low cost in free-energy which are very favoured entropically. In what follows we will see that this is the case of the directed polymer in random media. However, in the study of the REEM we will see that even in the absence of true chaos, κ_F can diverge when we are close to a localisation transition.

We have to note that this definition of chaos is valid also for other types of perturbation than temperature changes such as the introduction of a small uniform magnetic field. There is a consensus on the existence of chaos under this kind of perturbation, however the mechanism is different as we will see in the analysis of the DPRM. Despite the fact that different perturbations can lead to different decays of correlation functions, it is very remarkable that in replica space there exists a unified framework in which chaos acquires a definite meaning for any kind of perturbation.

1.1.1 The interpretation of chaos in replica space.

In systems which are suitable for replica analysis there can be introduced an equivalent definition of chaos. Let us suppose that each of the two copies A and B are replicated further into n replicas. From the disorder average of the replicated partition function $Z^n_{\mathrm{A+B}}(L)$ we can obtain the distribution function of sample-to-sample fluctuation of the free-energy. This is because when the analytical continuation to $n \to 0$ is possible [Kar96], $\overline{Z^n_{\mathrm{A+B}}(L)}$ can be identified with the generator of cumulant correlation functions of sample-to-sample fluctuations of the free-energy as follows,

$$\begin{aligned}
\lim_{n\to 0} \quad & \ln \overline{Z^n_{\mathrm{A+B}}(L)} \\
= \; & n\overline{\ln Z_{\mathrm{A+B}}(L)} + \frac{n^2}{2}\overline{[\ln Z_{\mathrm{A+B}}(L)]^2_c} + \ldots + \frac{n^p}{p!}\overline{[\ln Z_{\mathrm{A+B}}(L)]^p_c} + \ldots \\
= \; & n\overline{[-\beta_{\mathrm{A}} F_{\mathrm{A}}(L) - \beta_{\mathrm{B}} F_{\mathrm{B}}(L)]} + \frac{n^2}{2}\overline{[-\beta_{\mathrm{A}} F_{\mathrm{A}}(L) - \beta_{\mathrm{B}} F_{\mathrm{B}}(L)]^2_c}
\end{aligned}$$

$$+ \quad \ldots + \frac{n^p}{p!}\overline{[-\beta_A F_{\rm A} - \beta_B F_{\rm B}]_c^p} + \ldots \tag{5.13}$$

where $[\ldots]_c^p$ stands for p-th cumulant correlation functions of the total free-energies $-\beta_{\rm A} F_{\rm A} - \beta_{\rm B} F_{\rm B}$ with $F_{\rm A}(L)$ and $F_{\rm B}(L)$ being free-energies of subsystems A and B respectively and $\beta_{\rm A}$ and $\beta_{\rm B}$ being inverse temperatures of A and B respectively.

Obviously, the decorrelation of the free-energy fluctuations between A and B is equivalent to the factorisation of the replicated partition function, $\overline{Z^n_{\rm A+B}(L,\delta)} = \overline{Z^n_{\rm A}(L)} \times \overline{Z^n_{\rm B}(L)}$. Hence,

$$\lim_{\delta\to 0}\lim_{L\to\infty}\lim_{n\to 0} \qquad \frac{\ln[\overline{Z^n_{\rm A+B}(L,\delta)}]}{n} = \frac{\ln \overline{Z^n_{\rm A}(L)}}{n} + \frac{\ln \overline{Z^n_{\rm B}(L)}}{n} \tag{5.14}$$

Note that if the latter result holds, automatically (5.6) holds too. An important remark is that the order in which limits are taken is crucial to obtain sensible results: the limit $n \to 0$ *must be taken before than the thermodynamic limit* $L \to \infty$ and finally the limit $\delta \to 0$ must be taken [5]. We have to stress, that this definition of chaos is general and holds for generic random systems.

This definition implies that chaos can be regarded as a spontaneous symmetry breaking phenomenon. In the absence of an external perturbation, A and B are equivalent, so that one expects the exchange symmetry $\rm A \leftrightarrow B$ and also the permutation symmetry among the replicas in each group to be present. This is usually denoted as replica symmetry. Besides, it turns out that the disorder-averaged replicated partition function of the $2 \times n$ replicas $\overline{Z^n_{\rm A+B}}$ without any perturbation has an even higher symmetry: it is invariant under any permutation among the $2 \times n$ replicas. Now, if (5.14) holds, this higher symmetry is reduced: after having introduced a perturbation the permutation symmetry remains at most within each subset associated with A and B. Thus, the perturbation should show up in the replicated partition function as a symmetry breaking term which tries to break the full permutation symmetry. Therefore, because (5.14) tells us that this symmetry breaking happens even with an arbitrary weak perturbation, chaos is a spontaneous replica symmetry breaking phenomenon. Such a definition of replica symmetry breaking was introduced under the name *explicit replica symmetry breaking* first by Parisi and Virasoro [PV89] in an attempt to give a sound thermodynamic definition for the replica symmetry breaking phenomena found in the saddle point solutions of mean-field models [Par80, MPV87].

1.2 Response to temperature changes: a geometrical measure

One of the most interesting issues is to work out the mechanism which brings about the strong rejuvenation effects in dynamical quantities.

[5] Note that this is not the usual situation met in mean-field models where the limit $n \to 0$ has to be taken after having solved the saddle-point equations valid in the infinite-volume limit.

Specially in models defined in configuration space, it is useful to assign to each state $i \in [1, L]$ with energy ϵ_i an observable $\mathcal{O}_i$ independent from the energy of the state. For instance, in a model describing the position of the pinning centre of an interface, it can be the spatial position of the state, or in a spin system, the magnetisation of a certain spin configuration. The thermodynamical value of this observable is thus,

$$\langle \mathcal{O} \rangle = \frac{1}{\mathcal{Z}} \sum_i O_i \, z_i \, ; \qquad z_i \equiv \exp(-\beta \epsilon_i) \ . \tag{5.15}$$

We can then construct the following response function,

$$\mathcal{R}(\delta, \mathcal{O}) = \overline{\left(\langle \mathcal{O} \rangle_{\mathcal{H}^{\mathrm{A}}} - \langle \mathcal{O} \rangle_{\mathcal{H}^{\mathrm{B}}} \right)^2} \ . \tag{5.16}$$

In the case of the observable being the position $\mathcal{O}_i = x_i = i/L$ this is a geometrical way to visualise temperature chaos. Besides, this observable could be interesting in pulling experiments of DNA molecules where to each separation between the end points x of the two chains, there is a (free-)energy associated [LN01]. The study of the distance between average positions corresponding to different temperatures gives us an indication of the distance between states contributing to $\mathcal{Z}$ at different temperatures. If typical states contributing to $\mathcal{Z}$ at T_1 and T_2 are completely different, then $\mathcal{R}(\delta, x)$ will remain finite as $L \to \infty$. It can be proved that $\mathcal{R}(\delta, x)$ has an upper bound $\mathcal{R}(\delta, x) \leq 1/6$, where $1/6$ is the value reached if the occupied sites are completely uncorrelated [6].

For small temperature differences between A and B, $T_{\mathrm{A}} - T_{\mathrm{B}} = 2T\delta$. Hence, from the fluctuation-dissipation relation $\frac{\partial \langle O \rangle}{\partial \beta} = \beta \, \langle O \epsilon \rangle_c$ we obtain,

$$\mathcal{R}(\delta, \mathcal{O}) = \frac{(2\,\delta)^2}{T^2} \, \overline{\left(\langle \mathcal{O}\epsilon \rangle - \langle \mathcal{O} \rangle \langle \epsilon \rangle \right)^2} = \delta^2 \, \kappa_{\mathcal{O}} \, \overline{\left(\langle \mathcal{O} \rangle - \overline{\langle \mathcal{O} \rangle} \right)^2} \ , \tag{5.17}$$

where thermal averages are evaluated at the middle temperature T. Note that we have introduced the variance of the observable which scales as $\mathcal{R}$ in order to define an adimensional susceptibility, which we expect to diverge in the large-size limit if the system is chaotic.

2. The Directed Polymer in Random Media

The DPRM [HHZ95] is a simple model compared to spin-glass models.However, there exist, as well, gap-less excitations that bring about an anomalous response toward various kinds of weak perturbations [HHH93] including a signature of temperature-chaos [FH91b].

[6] Note that if positions are completely uncorrelated the weights are flat so that: $\overline{(x_{\mathrm{A}} - x_{\mathrm{B}})^2} = \int_0^L \frac{dy}{L} \int_0^L \frac{dx}{L} \frac{(x-y)^2}{L^2} = \frac{1}{6}$.

The DPRM is an elastic line in a disordered medium that in $1+1$ dimensions is described by the following Hamiltonian in the continuous limit (5.18),

$$H_0[V,h,\phi] = \int_0^L dz \left[\frac{\kappa}{2} \left(\frac{d\phi(z)}{dz} \right)^2 + V_0(\phi(z),z) \right]. \tag{5.18}$$

The scalar field ϕ represents the displacement of the elastic object at point z in a 1-dimensional internal space of size L. In the following, we assume that one end of the string is fixed as $\phi(0)=0$ while the other end $\phi(L)$ is allowed to move freely. κ is the elastic constant and the disorder is introduced by the quenched random potential $V_0(\phi,z)$ with zero mean and short-ranged spatial correlation $\overline{V_0(\phi,z)V_0(\phi',z')} = 2D\delta(\phi-\phi')\delta(z-z')$.

2.1 Droplet Scaling Approach

First we review and discuss the scaling approach picture [FH91b, HHH93] for the problem of the anomalous response.

The DPRM is characterised by having a very large (extensive with L) fluctuations of the ground-state end-point position. This is due to the existence of anomalously large excitations with a low free-energy cost $\Phi_L^{\rm typ} = U_0 L^\theta$, where U_0 is a the typical free-energy scale cost when $L=1$. One can depict the DP as a deep valley corresponding to the ground-state configuration and many branched valleys of low (free-)energy excitations which for given longitudinal size L differ from the 'ground state' over a transverse size L^ζ [7], ζ being the so called roughness exponent related with the stiffness exponent θ by the exact scaling relation, $\theta = 2\zeta - 1$.

In a $1+1$ dimensional system these exponents are believed to be exactly $\theta = 1/3$ and $\zeta = 2/3$ [HH85, HHZ95]. The probability distribution function of the free-energy gap Φ_L is expected to have a natural scaling form,

$$\rho_L(\Phi_L) d(\Phi_L) = \tilde{\rho}\left(\frac{\Phi_L}{U_0 L^\theta} \right) \frac{d(\Phi_L)}{U_0 L^\theta}, \tag{5.19}$$

with non-vanishing amplitude at the origin, $\tilde{\rho}(0) > 0$, allowing rare gap-less excited states [FH91b, Méz90]. These excitations will exist at any finite temperature T for large enough length scales with probability $\sim T/L^\theta$. These will dominate at large L over the contributions from the smaller scales and in particular from the typical fluctuations of order $L_T \sim T^{1/\theta}$, giving rise to anomalously large fluctuations of the DP around its ground state,

$$\overline{\left(\phi(L) - \overline{\phi(L)}\right)^2} \sim T\tilde{\rho}(0) L^{2\zeta-\theta} \quad . \tag{5.20}$$

[7] We note that L is here an adimensional length which stands for $L_{\rm real}/L_0$ where L_0 is the Larkin length [Lar70] beyond which pinning becomes important. The same is true for the transverse length scale associated to L, $L^\zeta = L^\zeta_{\rm real}/u_0$, with $u_0 = L_0^\zeta$.

The existence of such excitations is of much relevance in the existence of chaos. Consider a generic perturbation as expressed in (5.2) which triggers an excitation from the 'ground state' with a *free-energy gain* of order $\delta U\ L^{\alpha}$, when the perturbation is small $\delta U/U_0 \to 0$. If we consider perturbations such that $\alpha > \theta$, under the influence of such a perturbation, the system in the deepest valley may jump into other valleys with free-energy gap Φ if the possible gain of free-energy due to the perturbation becomes larger than the original free-energy gap itself. According to (5.19) the probability of such an event is estimated as,

$$p_{\rm jump}(L,\delta U) \sim \frac{\delta U L^{\alpha}}{U_0 L^{\theta}} = \left(\frac{L}{L_c(\delta U)}\right)^{\alpha-\theta}, \qquad L_c(\delta U) \sim \left(\frac{\delta U}{U_0}\right)^{-1/(\alpha-\theta)} \tag{5.21}$$

where we have defined a characteristic length scale called *overlap length* beyond which both DPs become uncorrelated introduced in (5.1). Note that $L_c(\delta)$ diverges as $\delta U/U_0 \to 0$ with exponent $-1/(\alpha-\theta)$, in (5.1) we have called this exponent ζ as is usual in spin glass problems. Here we do not use the convention because in this context ζ is usually used for the roughness exponent [8].

It is important to note that the above expressions make sense only for short enough length scales $L \ll L_c(\delta U)$. In this regime the effect of the jumps on physical quantities can be analysed in a perturbative way because the probability of a jump is small enough. Let us call this regime *weakly perturbed regime*. However, in *strongly perturbed regime* $L \gg L_c(\delta U)$, standard perturbative treatments will fail because jump events will happen with probability one.

2.1.1 Correlation Functions

In order to characterise the jump events triggered by the perturbations we have analysed the correlations of free-energy fluctuations through C_F as defined in 5.11. One can also study other correlation functions such as the overlap q and $\mathcal{B}_q$, the disorder average of the q-th moment of the transverse distance between the end points of the two real replicas, defined as,

$$q(L,\delta U) = \frac{1}{L}\overline{\sum_{z=1,L}\delta(\phi_{\rm A}(z)-\phi_{\rm B}(z))} \tag{5.22}$$

$$\mathcal{B}_q(L,\delta U) = \overline{(\phi_{\rm A}(L)-\phi_{\rm B}(L))^q}\ . \tag{5.23}$$

Nevertheless the information about the scalings and crossovers yield by these quantities is analogous to that given by C_F, so that we will focus our analysis in the latter [SY02].

What is interesting in this study is the fact that apart from giving arguments on the existence of chaos against any small perturbation for the DP [SY02] we can also give

[8] Note that in the same way we can define a characteristic length scale in transverse space which is conjugate to $L_c(\delta U)$, $u_c(\delta U) = u_0 L_c(\delta U)^{\zeta}$.

scaling arguments for the crossover to the strongly perturbed regime which will be confirmed by the numerics. Here we will investigate the behaviour of C_F for two different perturbation types a change in temperature and applied uniform magnetic field.

In virtue of the analysis made in Sec. 1.1 we expect C_F to be a scaling function of $L/L_c(\delta U)$ going to zero in the limit $L \to \infty$. And in particular from (5.12) we expect the following functional form for small perturbations,

$$1 - C_F \sim \left(\frac{L}{L_c}\right)^{2(\alpha-\theta)} \quad ; \qquad \frac{\delta U}{U_0} \to 0 \tag{5.24}$$

In the strongly perturbed regime $L \gg L_c(\delta)$, the correlation function may decay faster.

2.1.2 Perturbations

We shall consider two different types of perturbations: the introduction of a magnetic field and a change in temperature. The interesting point is that even though the system is sensible to both type of perturbations, the symmetries preserved by each perturbation are different. This leads to different exponents governing the divergence of the overlap length, and thus to different universality classes. This is the reflex of the different nature of the mechanisms leading to chaos in each case. Such a difference will become clearer in the replica analysis performed in Sec. 2.2.

- Uniform Tilt Field

  We first consider the application of a uniform tilt field h to the end-point of the real replica B at $z = L$ by which the statistical rotational symmetry is violated. In the presence of the tilt field the Hamiltonian becomes,

  $$H_{A+B} = H_0[V_0, \phi_{\rm A}] + H_0[V_0, \phi_{\rm B}] - h \int_0^L dz \frac{d\phi_B(z)}{dz} \tag{5.25}$$

  The unperturbed Hamiltonian H_0 is given in (5.18). If the string makes a jump responding to the uniform tilt field over a distance of order $u_0\ L^\zeta$ into the next valley, it obtains an energy gain of order $hu_0\ L^\zeta$ with characteristic exponent $\alpha = \zeta = 2/3$. Therefore we find the overlap length (5.1) to be [Méz90],

  $$L_c(h) \sim \left(\frac{hu_0}{U_0}\right)^{-3} \quad . \tag{5.26}$$

- Temperature Change

  The thermal perturbation does not break the translational symmetry present in the unperturbed Hamiltonian, but we will see that breaks the symmetry between replicas noted in Sec. 1.1.

  If we consider the introduction of a slight temperature difference between the two real replicas A and B , we expect that $\alpha = 1/2$ based on the following observation made

by Fisher and Huse [FH91b]. They conjectured that valley-to-valley fluctuations of the energy and the entropy are just that of a sum of random variables put on a string of length L. Thus the amplitude of these fluctuations scales as $\Delta S \sim L^{1/2}$ and $\Delta E \sim U_0 L^{1/2}$. However, it is argued that the free-energy is optimised so that these wild fluctuations of energy and entropy cancel out to yield much smaller valley-to-valley free-energy fluctuations, $\Phi(L) = U_0 L^{\theta}$ with $\theta < 1/2$. Such considerations can be confirmed numerically [FH91b]. Actually , the exponent for the free-energy fluctuations is believed to be exactly $\theta = 1/3$ which is smaller than $1/2$. A slight temperature-difference between the two replicas A and B, induces one of the two replicas to jump into a different valley taking advantage of the large gain in entropy. Such a gain should typically scale as $|\delta T| L^{1/2}$ and therefore $\alpha = 1/2$ and $\delta U \sim |\delta T|$. From (5.1), one then finds the overlap length as [FH91b],

$$L_c(\delta T) \sim \left(\frac{|\delta T|}{U_0} \right)^{-6} \quad . \tag{5.27}$$

Going back to the previous analysis of C_F for this particular perturbation, we recall that the susceptibility κ_F is proportional to the ratio between entropy and free-energy fluctuations so that,

$$\kappa_F = T^2 \frac{\overline{(\Delta S)^2}}{\overline{\Phi^2}} \sim T^2 \; L^{2(\alpha-\theta)} = T^2 \; L^{1/3} \quad . \tag{5.28}$$

Therefore for any finite temperature there is chaos in temperature, since κ_F diverges in the limit $L \to \infty$. Only exactly at $T = 0$ the susceptibility vanishes as expected from the fact that entropy vanishes.

As we have summarised previously, what is crucial is the role of entropy. In the so called Larkin model [Lar70], in which the effect of pinning is modelled by quenched random forces with short ranged correlations, entropy plays very little role and free-energy is dominated by energy so that there is no temperature-chaos (see [FLN91]), this is the case also of the Sinai model as we sill show in Sec. 4.

2.2 Replica Bethe Ansatz Approach

Now let us turn to the replica approach introduced in Sec. 1.1.1 to address the chaos problem. We start from the partition function of $2 \times n$ replicas: A and B and their n copies. It can be expressed by a path integral over all possible configurations of $2 \times n$ replicas labelled by two indexes $\mathrm{G} = \mathrm{A}, \mathrm{B}$ and $\alpha = 1, \ldots, n$,

$$\overline{Z^n_{\mathrm{A+B}}(L)} = \int \prod_{\mathrm{G=A,B}} \prod_{\alpha=1}^{n} \mathcal{D}\phi_{\mathrm{G},\alpha} \exp\left(-S_{\mathrm{A+B}}[\phi_{\mathrm{G},\alpha}]\right). \tag{5.29}$$

where we have introduced the dimension-less effective action,

$$S_{\mathrm{A+B}}[\phi_{\mathrm{G},\alpha}] = \int_0^L dz \left[\sum_{\mathrm{G},\alpha} \frac{\kappa}{2k_{\mathrm{B}}T} \left(\frac{d\phi_{\mathrm{G},\alpha}(z)}{dz} \right)^2 - \frac{D}{(k_{\mathrm{B}}T)^2} \sum_{\mathrm{G},\mathrm{G}',\alpha,\beta} \delta(\phi_{\mathrm{G},\alpha}(z) - \phi_{\mathrm{G}',\beta}(z)) \right] \tag{5.30}$$

To obtain the last equation we have used that the random potential has short range correlations.

The effective action (5.30) has several important symmetries. First, it has a symmetry under global rotation in the (z, ϕ) plane and second, it is symmetric under all possible permutations among the $2 \times n$ replicas. Let us call the latter as RS (replica symmetric) for simplicity. As we explained in Sec. 1.1.1 our primary interest is how the RS is broken by infinitesimally weak perturbations.

Now we focus on the study of the disorder averaged partition function $\overline{Z^n_{\mathrm{A+B}}(L)}$. In the absence of perturbations this problem can be solved by using the well-known mapping to an n-body imaginary time quantum mechanical problem in one dimension, as noted by Kardar [Kar87, Kar96]. The advantage of this approach is that one can find the exact ground state by means of the Bethe ansatz. Moreover, from the latter one gets many hints about how to construct the relevant excited states. In what follows the main steps in this procedure are outlined to emphasise several points which will become relevant in the analysis of the perturbation. The path-integral of the partition function defined in (5.29) through the action in (5.30) can be reinterpreted as that of a quantum system in imaginary time, with the longitudinal coordinate playing the role of time. In the absence of perturbations the Schrödinger equation reads,

$$-\frac{\partial}{\partial t} \overline{Z^n_{\mathrm{A+B}}(\{x_{\mathrm{G},\alpha}\}, t)} = \mathcal{H}_0 \overline{Z^n_{\mathrm{A+B}}(\{x_{\mathrm{G},\alpha}\}, t)} \quad , \tag{5.31}$$

with the following Schrödinger operator for $2 \times n$-bosons,

$$\mathcal{H}_0 = -\sum_{\mathrm{G},\alpha} \frac{k_{\mathrm{B}}T}{2\kappa} \frac{\partial^2}{\partial x^2_{\mathrm{G},\alpha}} - \frac{D}{(k_{\mathrm{B}}T)^2} \sum_{((\mathrm{G},\alpha),(\mathrm{G}',\beta))} \delta(x_{\mathrm{G},\alpha} - x_{\mathrm{G}',\beta}) \quad . \tag{5.32}$$

The 1st term represents the kinetic energy. The 2nd term stands for the attractive short-ranged interactions between all possible pairs of replicas (excluding unphysical self-interactions which are absent in lattice models). Let us note that even though we have two different groups of identical particles (*bosons*), A and B, the Schrödinger operator has an even higher bosonic symmetry: it is symmetric under permutations of all the $2 \times n$ replicas. Therefore, the ground state will contain this symmetry. This is nothing but the RS we mentioned above.

In the large L (large time) limit, the partition function will be dominated by the eigenstate of the Schrödinger operator with lowest eigenvalue (*energies*) including the ground state. The ground-state wave function is well-known to satisfy the Bethe ansatz reading [Kar87],

$$< \Psi_{\rm RS} | \{x_{{\rm G},\alpha}\} > \sim \exp\left(-\lambda \sum_{(({\rm G},\alpha),({\rm G}',\beta))} |x_{\alpha,{\rm G}} - x_{\beta,{\rm G}'}| \right) \tag{5.33}$$

where we have introduced $\lambda = \kappa D/(k_{\rm B}T)^3$ and the sum is taken over all possible pairs among the $2 \times n$ replicas labelled as $({\rm G}(={\rm A},{\rm B}), \alpha(=1,\ldots,n))$. The index RS stands for the fact that this wave function contains the permutation symmetry among all $2 \times n$-replicas. In the following we label this state as replica symmetric (RS). The ground-state energy is the sum of the kinetic energy of the $2 \times n$ *free-particles*,

$$E_{\rm g} = -\frac{k_{\rm B}T}{2\kappa} \sum_{m=1}^{2n} \lambda_m^2 = -\frac{k_{\rm B}T}{2\kappa} \frac{1}{3} \lambda^2 \, 2n(4n^2-1) \quad . \tag{5.34}$$

Although the ground state yields the most important contribution to the partition function, it may not be the only one. If one *only* takes into account the contribution of the ground state neglecting all other excited states, one would wrongly conclude from the only presence of term of order n and n^3 in (5.34) and the relation (5.13) that only the 1st and 3rd cumulants of the correlation functions of free-energy fluctuations exist. This conclusion is definitely unphysical because it can be shown that the 2nd cumulant cannot be zero. Such a pathology implies existence of continuum of gap-less excited states which give important contributions to the partition function.

Orland and Bouchaud [BO90] pointed out that the translational symmetry of the Schrödinger operator allows to construct a continuous spectrum of excited states with non-zero centre of mass moment. As we show in Sec. 2.3 the resultant partition function obtained by integrating out the continuous spectrum can be put into the following scaling form [Kar96],

$$\ln \overline{Z_{\rm A+B}^n} = -2n\beta \overline{f} L + g(2nL^{1/3}) \quad . \tag{5.35}$$

where $\overline{f}$ in the 1st term represents the average free-energy density. The function $g(x)$ in the 2nd term is analytic for small $x = 2nL^{1/3}$, implying that the q-th cumulant of the correlation function of free-energy fluctuations scales as $L^{q/3}$. Thus the characteristic exponent for the free-energy fluctuation, which is called stiffness exponent, is obtained as $\theta = 1/3$, being consistent with extensive numerical results of transfer matrix calculations [HHZ95] and other analytical approaches such as the mapping to the noisy Burgers equation [HHF85].

As Parisi [Par90] pointed out one can construct other excited states in which replicas are grouped into *clusters* of bound states. Each cluster is described by a Bethe ansatz type wave function so that there is replica (permutation) symmetry within each cluster.

An important assumption is that these clusters are located far enough from each other so that their mutual overlap is negligible. The latter is allowed if the transverse size of the system is infinitely large.

In the present context, this means considering an excited state that consists of two separate Bethe type clusters $< \Psi^{\rm A}_{\rm RS}|$ and $< \Psi^{\rm B}_{\rm RS}|$, with no mutual overlap,

$$< \Psi_{\rm RSB}| =< \Psi^{\rm A}_{\rm RS}| \times < \Psi^{\rm B}_{\rm RS}| \, ; \qquad < \Psi^{\rm B}_{\rm RS}|\Psi^{\rm A}_{\rm RS} >= 0, \tag{5.36}$$

whose associated energy is readily obtained as twice the energy of a single Bethe cluster,

$$E_{\rm RSB} = -\frac{k_{\rm B}T}{2\kappa}\frac{1}{3}\,\lambda^2\,n\left(n^2-1\right)\times 2. \tag{5.37}$$

This wave function has the reduced replica symmetry mentioned before, *i.e.* it is symmetric under permutations among A and B groups and the exchange operation $A \leftrightarrow B$. We will call this state as replica symmetry broken (RSB) state in the following.

The important point here is that the gap with respect to the true ground state is of order $O(n^3)$ and thus vanishes in the $n \to 0$ limit. Thus such an excited state should be also taken into account since we must take $n \to 0$ before $L \to \infty$ in the evaluation of the replicated partition function. Presumably each cluster of bound states can have its own centre of mass motion, and therefore it should have the continuum of excited states of CM motion similar to that associated with the RS ground state mentioned above. Then the resultant partition function $\overline{Z^n_{A+B}}$ may be put again into the scaling form (5.35), yielding $\theta = 1/3$.

To sum up, replica symmetry is not strictly broken but it is so in a *marginal* way. As suggested by Parisi [Par90], the role of these RSB excited states will become important if perturbations are considered. In the following we generalise the approach of [Par90] and exploit its implications to study the stability of the frozen phase against the perturbations considered in Sec. 2.1.

2.2.1 A Perturbative Approach by Replica Scaling Ansatz

Now we address the situation in which the two real replicas A and B are under infinitesimally weak perturbations. The partition function of the system under such a perturbation can be formally written as,

$$\overline{Z^n_{\rm A+B}(L)} = \int \prod_{\rm G=A,B}\prod_{\alpha=1}^{n} \mathcal{D}\phi_{{\rm G},\alpha}\, \exp\left(-S_{\rm A+B}[\phi_{{\rm G},\alpha}] - \delta S_{\rm A+B}[\phi_{{\rm G},\alpha}]\right). \tag{5.38}$$

Above, the action $S_{\rm A+B}[\phi_{G,\alpha}]$ is the original one (5.30), which is fully replica symmetric, and the 2nd one $\delta S_{\rm A+B}[\phi_{{\rm G},\alpha}]$ is the perturbation term.

Suppose that we can map the problem onto a quantum mechanical one such that the corresponding Schrödinger operator becomes,

$$\mathcal{H}_{\rm A+B} = \mathcal{H}_0 + \delta\mathcal{H} \tag{5.39}$$

where $\mathcal{H}_0$ is the original fully replica symmetric $2 \times n$-boson operator given in (5.32) and $\delta\mathcal{H}$ corresponds to δS in the path-integral. As we will see in the following, these perturbations try to break the RS present in the original system down to the reduced symmetry: replica symmetric only within A and B subgroups. At this stage, the whole quantum problem can not be solved exactly. However, we can obtain a useful insight into our problem by a perturbation analysis as proposed by Parisi [Par90].

From standard perturbation theory we can evaluate the first order corrections to the original ground-state energy as,

$$E_{\Delta}^{\mathrm{RS}} = -\frac{1}{3}\frac{k_{\mathrm{B}}T}{2\kappa}\,\lambda^2\,2n(4n^2-1) + \frac{\langle\Psi_{\mathrm{RS}}|\delta\mathcal{H}|\Psi_{\mathrm{RS}}\rangle}{\langle\Psi_{\mathrm{RS}}|\Psi_{\mathrm{RS}}\rangle} \quad , \tag{5.40}$$

where the label Δ stands for the perturbation strength and $\langle\Psi_{\mathrm{RS}}|$ is the ground-state wave function given in (5.33). The 1st term corresponds to the ground-state energy given in (5.34).

Following Parisi, we will consider the RSB excited state (5.36). At 1st order in perturbation theory, we can compute the energy of the RSB excited states as follows,

$$E_{\Delta}^{\mathrm{RSB}} = -\frac{1}{3}\frac{k_{\mathrm{B}}T}{2\kappa}\,\lambda^2\,2n(n^2-1) + \frac{\langle\Psi_{\mathrm{RSB}}|\delta\mathcal{H}|\Psi_{\mathrm{RSB}}\rangle}{\langle\Psi_{\mathrm{RSB}}|\Psi_{\mathrm{RSB}}\rangle} \quad , \tag{5.41}$$

where the 1st term is the energy of the unperturbed system given by (5.37).

Let us introduce the difference of the contributions to the partition function $\overline{Z_{A+B}^n}$ due to the RS ground state and the RSB excited state,

$$D(n,L) \equiv (E_{\Delta}^{\mathrm{RSB}} - E_{\Delta}^{\mathrm{RS}})L = D_0(n,L) - \delta D(n,L) \tag{5.42}$$

where

$$D_0(n,L) = \frac{k_{\mathrm{B}}T}{\kappa}\,\lambda^2\,n^3L \qquad > 0 \tag{5.43}$$

is the original 'energy gap' and the correction is due to the 1st order perturbation,

$$\delta D(n,L) = L\left(\frac{\langle\Psi_{\mathrm{RSB}}|\delta\mathcal{H}|\Psi_{\mathrm{RSB}}\rangle}{\langle\Psi_{\mathrm{RSB}}|\Psi_{\mathrm{RSB}}\rangle} - \frac{\langle\Psi_{\mathrm{RS}}|\delta\mathcal{H}|\Psi_{\mathrm{RS}}\rangle}{\langle\Psi_{\mathrm{RS}}|\Psi_{\mathrm{RS}}\rangle}\right). \tag{5.44}$$

In the following we use the term gap to refer to $D(n,L)$. If it is large enough, the contribution of the RSB excited state to the partition function becomes negligible. We will find that, in general, the correction term of the gap has the form,

$$-\delta D(n,L) = -\Delta n^p L < 0. \tag{5.45}$$

Here the symbol Δ stands for the strength of the perturbation. In general, the correction term $-\delta D(n,L)/L$ is polynomial in n but the term which becomes most relevant in the $n \to 0$ limit is the one with smallest exponent p which hereafter we will call *order of the perturbation*. Most importantly, $-\Delta n^p$ will turn out to be *negative* for all the

perturbations under consideration, which means that the introduction of a perturbation results in a gain of (free-)energy.

If the 1st order correction vanishes, we would have to proceed to higher order perturbation calculations which is not possible without the complete knowledge of the whole spectrum of excited states. This is the case of the uniform tilt field, however we have been able to find exact RS and RSB bound states of the system which will allow the evaluation of the gap $D(n, L)$ also in this situation. In the other cases, we expect that higher order correction terms will be of $\mathcal{O}(\Delta^2)$ and therefore irrelevant in the limit $\Delta \to 0$. Since it is unlikely that the higher order terms are lower orders of n, these will be also irrelevant in the $n \to 0$ limit.

Substituting relations (5.45) and (5.43) in (5.42) we can express the gap as follows,

$$D(n, L) = D_0(n, L) \left[1 - \left(\frac{n}{n^*(\Delta)} \right)^{-(3-p)} \right] \tag{5.46}$$

with

$$n^*(\Delta) = \left(\frac{\Delta}{\lambda^2 k_{\rm B} T/\kappa} \right)^{1/(3-p)} \quad . \tag{5.47}$$

As long as n is integer and the strength of the perturbation Δ is small, the contribution of the RSB state becomes negligible in the thermodynamic limit $L \to \infty$ [9]. However, we have to consider the other limiting case: the $n \to 0$ limit should be taken before $L \to \infty$. Now if $p < 3$, which will turn out to be the case for all the perturbations under study, an arbitrarily small perturbation Δ will induce a level crossing at $n^*(\Delta)$ below which the contribution of the RSB excited state becomes larger than that of the original RS ground state. The result (5.46) matches perfectly with our definition of chaos (5.14) since it suggests that the partition function of the total system factorises in the $n \to 0$ limit,

$$\lim_{n/n* \to 0} \overline{Z^n_{\rm A+B}} = \overline{Z^n_{\rm A}} \times \overline{Z^n_{\rm B}} \qquad \text{if } p < 3. \tag{5.48}$$

implying a complete change of the free-energy landscape.

Now let us further exploit from the above result to find a more physical picture. In the absence of perturbations, the logarithm of the replicated partition function has a functional form (5.35) which reads as, $\ln \overline{Z^n_{A+B}} = -\beta \overline{f} L(2n) + g(2nL^{1/3})$. On the other hand, (5.46) implies that n/n^* is another natural variable of the replicated partition function [10]. Combining the two, we conjecture the following scaling ansatz,

$$\ln \overline{Z^n_{A+B}} + \beta \overline{f} L(2n) = \tilde{g}(2nL^{1/3}, n/n^*) = \tilde{g}(2nL^{1/3}, L/L^*) \quad . \tag{5.49}$$

[9] This is a generalisation of an argument used by Parisi in [Par90] for the explicit repulsive case ($p = 1$) to extract the following conclusions.

[10] To treat the replica number n as a scaling variable has been proposed by several authors [HHZ95, Kar96, EK01].

where we introduced a characteristic length L^* defined as,

$$L^* \sim (n^*)^{-3} \sim \Delta^{-3/(3-p)} \tag{5.50}$$

An interesting observation is that if the variable $nL^{1/3} = x$ is fixed, the limit $n \to 0$ induces the thermodynamic limit $L \to \infty$. Then at fixed x we expect,

$$\begin{aligned} \tilde{g}(x, L/L^* \to 0) &\simeq g(2x) \qquad L/L^* \ll 1 \qquad (n/n^* \gg 1) \\ &\qquad\qquad \text{'weak perturbation regime'} \\ \tilde{g}(x, L/L^* \to \infty) &\simeq 2 \times g(x) L/L^* \gg 1 \qquad (n/n^* \ll 1) \\ &\qquad\qquad \text{'strong perturbation regime'}. \end{aligned} \tag{5.51}$$

The 1st equation means that for small enough length scales, the effect of the perturbation is small and the partition function is essentially the same as that of the unperturbed system of $2 \times n$-replicas given in (5.35). The 2nd equation is the consequence of having two statistically independent systems in the limit $L \to \infty$.

From the above scaling ansatz, it follows that the correlation function of the free-energy fluctuations $C_F(L)$ should have the scaling form $\tilde{C}_F(L/L^*)$ which goes to 0 as $L/L^* \to \infty$ [11].

Thus the crossover length L^* should be identified with the overlap length $L_c(\delta U)$. The above ansatz implies that the decorrelation of the free-energy landscape between A and B takes place as a universal phenomenon whose features are classified according to the order of the perturbation p. In the following, we consider the temperature shift and uniform tilt perturbations and evaluate the correction to the gap (5.45) explicitly and extract the strength of perturbation Δ and the order of perturbation p. Moreover, we recover the same overlap length obtained via real-space scaling arguments in the previous section.

The perturbations considered are such that the original symmetry is preserved as much as possible : the $2 \times n$-replica system remains invariant at least under permutations among the n-replicas belonging to the same subset A and B and the exchange A $\leftrightarrow$ B, *i. e.* the reduced replica symmetry.

2.2.2 Temperature Change

We have two real replicas in the same quenched random potential $V(\phi(z), z)$ that are subjected to a small temperature difference. The Schrödinger operator for the $2 \times n$-replica system with A at temperature $T_{\rm A}$ and B at temperature $T_{\rm B}$ is the following,

$$\begin{aligned} \mathcal{H} &= -\sum_{\alpha} \frac{k_{\rm B} T_{\rm A}}{2\kappa} \frac{\partial^2}{\partial x_{{\rm A},\alpha}^2} - \sum_{\alpha} \frac{k_{\rm B} T_{\rm B}}{2\kappa} \frac{\partial^2}{\partial x_{{\rm B},\alpha}^2} \\ &- \sum_{(({\rm G},\alpha),({\rm G}',\beta))} \frac{D}{(k_{\rm B} T_{\rm G})(k_{\rm B} T_{\rm G'})} \delta(x_{{\rm G},\alpha} - x_{{\rm G}',\beta}) \quad . \end{aligned} \tag{5.52}$$

[11] The scaling in L/L^* applies for all correlation functions such as the overlap q and $\mathcal{B}_q$ defined in (5.23) [SY02].

RS is apparently lost in the operator, but for small symmetric temperature shift $T_{\rm A/B} = T(1 \pm \delta),\ \delta \to 0$ we can put the operator in the form,

$$\mathcal{H} = \mathcal{H}_0 + \delta\mathcal{H}, \tag{5.53}$$

where $\mathcal{H}_0$ is given in (5.32) and the symmetry breaking terms are the following,

$$\begin{aligned}\delta\mathcal{H} = \quad & -\delta \sum_{\alpha} \frac{k_{\rm B}T}{2\kappa} \frac{\partial^2}{\partial x_{{\rm A},\alpha}^2} + 2\ \delta\ \sum_{\alpha,\beta} \frac{D}{(k_{\rm B}T)^2} \delta(x_{{\rm A},\alpha} - x_{{\rm A},\beta}) \\ & +\delta \sum_{\alpha} \frac{k_{\rm B}T}{2\kappa} \frac{\partial^2}{\partial x_{{\rm B},\alpha}^2} - 2\ \delta\ \sum_{\alpha,\beta} \frac{D}{(k_{\rm B}T)^2} \delta(x_{{\rm B},\alpha} - x_{{\rm B},\beta}) \\ & +2\ \delta^2 \sum_{\alpha,\beta} \frac{D}{(k_{\rm B}T)^2} \delta(x_{{\rm A},\alpha} - x_{{\rm B},\beta}) + \mathcal{O}\left(\delta^3\right). \end{aligned} \tag{5.54}$$

Since RS and RSB wave functions are symmetric with respect to the change $\mathrm{A} \leftrightarrow \mathrm{B}$, the expectation value of the perturbing operator is of order δ^2. Computing explicitly the expectation value of the delta-interaction term with respect to the Bethe ground state one obtains [Par90],

$$\frac{\langle \Psi_{\rm RS} | \delta(x_{{\rm A},\alpha} - x_{{\rm B},\alpha}) | \Psi_{\rm RS} \rangle}{\langle \Psi_{\rm RS} | \Psi_{\rm RS} \rangle} = \frac{\lambda}{6}\,(2n+1), \tag{5.55}$$

while for the RSB states the correction term vanishes because the bound states of A and B subsets have no overlap $\langle \Psi_{\rm RSB}^{\rm A} | \Psi_{\rm RSB}^{\rm B} \rangle = 0$ (5.36),

$$\frac{\langle \Psi_{\rm RSB} | \delta(x_{{\rm A},\alpha} - x_{{\rm B},\alpha}) | \Psi_{\rm RSB} \rangle}{\langle \Psi_{\rm RSB} | \Psi_{\rm RSB} \rangle} = 0. \tag{5.56}$$

Therefore, we obtain that the correction to the gap reads,

$$-\frac{\delta D(n,L)}{L} = -\frac{\lambda}{6} \frac{D}{(k_{\rm B}T)^2} (2n+1) \times 2 \left(\frac{\delta T}{T}\right)^2 \times n^2\ . \tag{5.57}$$

Note that this expression is invariant under the exchange $\mathrm{A} \leftrightarrow \mathrm{B}$, which is possible thanks to the anti-symmetric change in temperature. From the above results, we read off that the order of the perturbation is $p = 2$ and the strength of the perturbation is $\Delta \sim (\delta T)^2$. Hence, introducing this information in (5.50) yields the same crossover length found in the real-space-scaling approach (5.27): $L^* \sim (\delta T)^{-6}$.

Notably, applying a random field or perturbing the actual value of the random potential preserves the same symmetries and is a perturbation of the same order $p = 2$ implying that they belong to the same universality class [SY02]. In spin glasses the situation seems to be different. Except for MKRG spin glasses [BB87], numerical simulations show that bond perturbations lead to a fast decay of the correlations whereas temperature differences result in a much slower decorrelation (if ever reaching total decorrelation).

This could be either due to the fact that the symmetry breaking term in the action is of higher order or to the fact that the amplitude of the perturbation term is very small, as happens in the SK model [CR02b]. In the following section that in the DPRM magnetic field perturbations are more effective because they have a smaller chaos exponent, in agreement with the observations made in spin glass systems.

2.2.3 Uniform Tilt Field

Finally we consider the application of a uniform tilt h to one real replica and $-h$ to the other. The corresponding Schrödinger operator of the quantum mechanical problem reads as,

$$\begin{aligned}\mathcal{H} = & - \sum_{\mathrm{G},\alpha} \frac{k_{\mathrm{B}}T}{2\kappa} \frac{\partial^2}{\partial x_{\mathrm{G},\alpha}^2} - \frac{D}{(k_{\mathrm{B}}T)^2} \sum_{\mathrm{G},\mathrm{G}',\alpha,\beta} \delta(x_\alpha - x_\beta) \\ & - \frac{h}{\kappa} \sum_\alpha \frac{\partial}{\partial x_{\mathrm{A},\alpha}} + \frac{h}{\kappa} \sum_\alpha \frac{\partial}{\partial x_{\mathrm{B},\alpha}} \quad . \end{aligned} \tag{5.58}$$

Note that the first two terms are the original operator $\mathcal{H}_0$ given in (5.32). Here not only the full permutation symmetry among the $2 \times n$ replicas but also the global rotational symmetry is lost due to the field. Thus the universality of this perturbation should be very different from the ones discussed so far.

Now let us analyse the change of the RS state (5.33). One can easily see that the 1st order perturbation vanishes simply because the total "momentum" of the ground state is zero. On the other hand, one can also easily note that when a field is applied, the original wave function is no longer an eigenstate. Fortunately, the exact eigenstate can be found in this odd situation in which particles belonging to different subsets (A and B) are driven into opposite directions. The former Schrödinger operator (5.58) can be rewritten into the fully symmetric form of the original problem (5.32) by shifting the momenta as follows,

$$\frac{\partial}{\partial x'_{\mathrm{A},\alpha}} = \frac{\partial}{\partial x_{\mathrm{A},\alpha}} - \frac{h}{k_{\mathrm{B}}T} \, ; \qquad \frac{\partial}{\partial x'_{\mathrm{B},\alpha}} = \frac{\partial}{\partial x_{\mathrm{B},\alpha}} + \frac{h}{k_{\mathrm{B}}T} \quad . \tag{5.59}$$

Note that this transformation preserves the commutation relations between conjugated coordinates and moments (i.e. $[\frac{\partial}{\partial x'_{\mathrm{G},\alpha}} \, , x'_{\mathrm{G},\alpha}] = [\frac{\partial}{\partial x_{\mathrm{G},\alpha}} \, , x_{\mathrm{G},\alpha}]$). In terms of these new coordinates the RS ground state again takes the form of the Bethe Ansatz solution of (5.33). And, therefore, the final ground state can be obtained from Bethe's wave function by undoing the previous shifting of moments,

$$\Psi \sim \Psi_{\mathrm{RS}}(\{x_{\mathrm{G},\alpha}\}) \exp\left(\frac{h}{k_{\mathrm{B}}T} \sum_\alpha x_{\mathrm{A},\alpha}\right) \exp\left(-\frac{h}{k_{\mathrm{B}}T} \sum_\alpha x_{\mathrm{B},\alpha}\right) \quad , \tag{5.60}$$

where $\Psi_{\mathrm{RS}}(\{x_{G,\alpha}\})$ is the original Bethe ansatz wave function for $2 \times n$ replicas given in (5.33). The eigenvalue E_h corresponding to this wave function is obtained as,

$$E_h = E_0 + \frac{nh^2}{\kappa k_{\mathrm{B}}T} \quad . \tag{5.61}$$

Here E_0 is the original ground-state energy $E_{\rm g}$ given in (5.34). Although the original full permutation symmetry is lost in the wave function (5.60), it still describes a sort of bound state of $2 \times n$-particles. So we may refer to it as RS state. In the next subsection, we will discuss the mapping onto the Sinai model and the physical meaning will become clearer. The 2nd term of (5.61) gives the change of the eigenvalue of the RS state due to the perturbation $\Delta E_{\rm RS} = nh^2/(\kappa k_{\rm B}T)$.

Next let us consider the change of the eigenvalue corresponding to the RSB excited state which again is formed by two separate bound states for A and B subsets. Here it is useful to note that if *all* the particles are subjected to the common field, the unperturbed single-bound-state wave function is still an eigenstate of the operator. Based on this observation, it follows that the reasons why the unperturbed RSB wave function is still a valid eigenstate are twofold: *i)* there is no overlap between A and B and *ii)* rotational and replica symmetries are preserved within the same subsets. Thus the eigenvalue of the RSB state does not change by the perturbation, then $\Delta E_{\rm RSB} = 0$.

Using the above values of $\Delta E_{\rm RS}$ and $\Delta E_{\rm RSB}$ we obtain,

$$-\frac{D(n,L)}{L} = -\frac{nh^2}{\kappa k_{\rm B}T}. \tag{5.62}$$

We can now read off $p = 1$ and $\Delta \sim h^2$, which yields the overlap length $L_c \sim h^{-3}$. Then using (5.50) we find the same overlap length $L^* \sim h^{-3}$ that is consistent with the result (5.26) of the real-space scaling argument.

2.3 Mapping to a modified Sinai Model

In the previous section we have shown how the crossover from a weakly perturbed regime to a strongly (chaotic) perturbed regime can be interpreted in replica space as a crossing of levels corresponding to RS and RSB states. Here we aim at showing how chaos is explicitly realised in the decoupling of the energy landscape of two different replicas.

Specifically, we analyse the uniform tilt case and we use the well-known mapping to the Sinai model (see Sec. 4). to obtain an effective one-dimensional energy landscape for the free end $x(L)$. We derive this mapping by considering the spectrum of excited states $\{\psi_k\}$ generated by adding non-zero CM motion to the wave functions given in (5.60) and (5.36) for the RS and RSB cases. The former is supposed to describe the weakly perturbed regime $L \ll L_c(h)$ while the latter represents the strongly perturbed regime $L \gg L_c(h)$. In order to interpolate between the two limits, one can use a phenomenological model using a bounded Sinai potential.

Calculations can be made following Bouchaud and Orland [BO90] and are described in Appendix D. The idea is that the partition function of the $2n$ replicas can be exactly computed from the excited states described above. These $\{\psi_k\}$ are eigenfunctions of the Hamiltonian with eigenvalue E_k. The resulting free-energy has two contributions: the

ground-state (free-)energy $F_{\rm GS}$ and the term accounting for fluctuations,

$$\overline{Z(0,0|x_{\rm A},x_{\rm B})}=\sum_k e^{-E_k}\langle 00|\psi_k\rangle\langle\psi_k|x_{\rm A},x_{\rm b}\rangle\sim e^{-\beta F_{\rm GS}}\times\overline{[e^{-E_{\rm eff}}]}_{\mathcal{V}}\ . \tag{5.63}$$

The free-energy fluctuations depend on an effective Hamiltonian in terms of the magnetic field h, the end-point position x and a random potential defined at the end point of the polymer $\mathcal{V}(x(L))$. By means of defining the following rescaled variables,

$$x=L^{2/3}y\,,\ \ \mathcal{V}(x)=L^{1/3}\tilde{\mathcal{V}}(y)\,,\ \ h=L^{-1/3}\tilde{h}\ , \tag{5.64}$$

the effective Hamiltonian can be put into the form $E_{\rm eff}=nL^{1/3}\tilde{E}_{\rm eff}$, meaning that fluctuations scale as $L^{1/3}$ as expected. From the above scaling relation it follows that the effective Hamiltonian has long-ranged correlations in transverse space equivalent to those of the Sinai potential,

$$\overline{[(\tilde{\mathcal{V}}(y)-\tilde{\mathcal{V}}(y'))^2]}_{\tilde{\mathcal{V}}}\propto|y-y'|\ \ . \tag{5.65}$$

- Replica Symmetric case: $L<<L_c(h)$
  Here we construct the excited state wave function by adding centre of mass motion to the ground-state wave function under a uniform tilt (5.60),

$$\begin{aligned}&\Psi_{\rm RS}(h,k;\{x_{{\rm G},\alpha}\})\\&\sim\Psi_{\rm RS}(\{x_{G,\alpha}\})e^{\left[\frac{h}{k_{\rm B}T}\left(\sum_\alpha x_{A,\alpha}-\sum_\alpha x_{B,\alpha}\right)\right]}e^{\left(ik\sum_{G,\alpha}x_{G,\alpha}\right)}.\end{aligned} \tag{5.66}$$

  Within this ansatz the effective Hamiltonian in terms of rescaled variables given in (5.64) reads,

$$\begin{aligned}E_{\rm RS-Sinai}(T,h,\mathcal{V};y_{\rm A},y_{\rm B})=&\frac{\kappa}{2k_{\rm B}T}\frac{(y_{\rm A}+y_{\rm B})^2}{2}\\&+\tilde{\mathcal{V}}(y_{\rm A})+\tilde{\mathcal{V}}(y_{\rm B})-\frac{\tilde{h}}{k_{\rm B}T}y_{\rm A}+\frac{\tilde{h}}{k_{\rm B}T}y_{\rm B}\qquad.\end{aligned} \tag{5.67}$$

  By increasing $nL^{1/3}$, the partition function will be dominated by the minimum of the effective Hamiltonian $E_{\rm RS-Sinai}(T,h,\mathcal{V};y_{\rm A},y_{\rm B})$. Then the following physical interpretation can be made: the end points of the strings A and B are subjected to the *same effective quenched random potential* which has the same long-ranged correlations in transverse space as the Sinai model. There are two competing effects: an effective Hookian spring acting on the CM which tries to bind together the two real replicas and the transverse force due to the uniform field that pulls the two end points in opposite directions and increases with L (at fixed h).

- RSB case, $L >> L_c(h)$
  In this case, the two groups of replicas are assumed to be non-interacting. Thus, we consider the spectrum of excited states where each group A, B is described by an independent Bethe cluster with its own CM motion,

$$\begin{aligned} \Psi_{\mathrm{RSB}}(h, k_{\mathrm{A}}, k_{\mathrm{B}} : \{x_{\mathrm{G},\alpha}\}) &\sim \Psi_{\mathrm{RS}}(\{x_{\mathrm{A},\alpha}\})\Psi_{\mathrm{RS}}(\{x_{\mathrm{B},\alpha}\}) \\ &\times \exp\left(ik_{\mathrm{A}}\sum_{\alpha} x_{\mathrm{A},\alpha}\right)\exp\left(ik_{\mathrm{B}}\sum_{\alpha} x_{\mathrm{B},\alpha}\right). \end{aligned} \tag{5.68}$$

  The partition function can be computed to find the following rescaled effective Hamiltonian,

$$\begin{aligned} E_{\mathrm{RS-Sinai}}(T, h, \tilde{\mathcal{V}}_{\mathrm{A}}, \tilde{\mathcal{V}}_{\mathrm{B}}; y_{\mathrm{A}}, y_{\mathrm{B}}) = &\frac{\kappa}{2k_{\mathrm{B}}T}y_{\mathrm{A}}^2 + \tilde{\mathcal{V}}_{\mathrm{A}}(y_{\mathrm{A}}) - \frac{\tilde{h}}{k_{\mathrm{B}}T}y_{\mathrm{A}} \\ &+\frac{\kappa}{2k_{\mathrm{B}}T}y_{\mathrm{B}}^2 + \tilde{\mathcal{V}}_{\mathrm{B}}(y_{\mathrm{B}}) + \frac{\tilde{h}}{k_{\mathrm{B}}T}y_{\mathrm{B}} \end{aligned} \quad .(5.69)$$

  It is interesting to compare the last result with the replica symmetric (RS) one given in (5.67). Here the two subsets A and B are now subjected to *independent Hookian springs* which try to confine the CM of each subset while the *total* CM was confined in the RS case. Moreover, the two replicas are now subjected to *completely independent Sinai potentials* $\tilde{\mathcal{V}}_{\mathrm{A}}$ and $\tilde{\mathcal{V}}_{\mathrm{B}}$. Again, the effect of the uniform tilt field amounts to an effective transverse force $\tilde{h}$ applied at the end points of both replicas trying to drive them in opposite directions just as in the replica symmetric case.

- A phenomenological model for the crossover.
  In Sec. 2.2, we conjectured a possible scaling form (5.49) of the crossover from the weakly perturbed regime at length scales shorter than the overlap length L_c where the RS holds, to the strongly perturbed regime where replica symmetry breaking becomes relevant,

$$\ln \overline{Z^n_{\mathrm{A+B}}} + \beta\overline{f}L(2n) = \tilde{g}(2nL^{1/3}, L/L_c) \quad . \tag{5.70}$$

  Indeed, the partition functions based on the RS and RSB ansätze have the expected form: the $O(n)$ term which provides the average free-energy $\beta\overline{f}L(2n)$ plus a function which contains the two scaling variables $nL^{1/3}$ and $\tilde{h} = L^{1/3}h = (L/L_c(h))^{1/3}$. In the last equation we have used the relation $L_c(h) \sim h^{-3}$ given in (5.26).

  Nevertheless, the crossover between the two limits remains an open problem. Here we propose a modified Sinai model which interpolates between the limits. At length L the modified Hamiltonian reads,

$$H = H_A + H_B \qquad \left\{ \begin{array}{rcl} H_A &=& \frac{\kappa}{2k_{\mathrm{B}}T}y_A^2 + \tilde{\mathcal{V}}(y_A) + \tilde{h}\ y_A \\ H_B &=& \frac{\kappa}{2k_{\mathrm{B}}T}y_B^2 + \tilde{\mathcal{V}}(y_B) - \tilde{h}\ y_B \end{array} \right. \tag{5.71}$$

where $\tilde{\mathcal{V}}(x)$ is a *bounded* Sinai potential with correlations,

$$\overline{(\tilde{\mathcal{V}}(x) - \tilde{\mathcal{V}}(y))^2} \propto C(|x-y|) \text{ with } C(u) = y + (1-u)\theta(u-1) \tag{5.72}$$

Here the correlation grows as $C(u) = u$ for $u \leq 1$ and saturates $C(u) = 1$ for larger separations $u > 1$. This saturation is equivalent to having a confined random walk and allows to realise statistically independent Sinai valleys at large separations (RSB). Actually such a saturation of the effective energy landscape was observed numerically in the DPRM by Mézard [Méz90].

In Sec. 2.4.1 we analyse the crossover phenomena in detail by a transfer matrix method and we compare it with the numerical results obtained with the modified Sinai model defined above .

2.4 Numerical Analysis

In this section, we examine numerically by transfer matrix calculations the properties of the anomalous response of the DPRM toward various perturbations discussed in the previous sections. We focus on the anticipated universal scaling properties of the crossover from the weakly to the strongly perturbed regime through the overlap length which has not been clarified in previous numerical studies (see however [Méz90]).

First we prepare two real replicas A and B identically except from small perturbations which we will describe in detail. Depending on the type of problem, we use either the zero-temperature [HH85] or the finite-temperature versions [Kar85] of the transfer matrix method to compute the correlation functions. Then we compute the exact free-energies (or ground-state energies at zero temperature) of both replicas and examine the correlation of the free-energies C_F defined in (5.5).

Numerical details: Specifically, we consider a lattice model on a two-dimensional lattice of size $L \times U$ as shown in Fig. 5.1. The string of length L is directed along the z axis with transverse displacements in the direction of the u-axis. The configuration of the string is represented by the positions of the vertexes "X" in which the configuration goes through, *i. e.* $(u(z), z)$ with $z = 1, \ldots, L$. The "gradient" $\sigma(z) = u(z+1) - u(z)$ is constrained to take only the values $+1$ or -1. Note that elasticity is realised entropically within this lattice model an thus it does not contribute to H. The random potential $V(u, z)$ is defined on each vertex (u, z) on which it takes a random value drawn from a uniform distribution between $-V_0$ and V_0. The energy of a configuration $\{u(z)\}$ is thus $E[V, u] = \sum_{z=1}^{L} V(u(z), z)$. One end of the configuration is fixed at $(0, 0)$ and the other end is allowed to move freely. On the transverse direction we have imposed periodic boundary conditions such that $V(u + U, z) = V(u, z)$ [12].

We have examined various system sizes up to $L = 10^4$ and have averaged over $N_s = 10^4$ different realisations of the random potential. We have used the following parameters for each perturbation: *a)* uniform tilt perturbation: we have used the $T = 0$ transfer matrix method and obtained the ground

[12] The natural unit for the temperature is the scaled thermal energy $k_B T/V_0$ where V_0 is the unit for the random potential. In the following, the Boltzmann's constant is set to $k_B = 1$ and the unit for the random potential to $V_0 = 1$, so that we will often denote the scaled thermal energy simply as T.

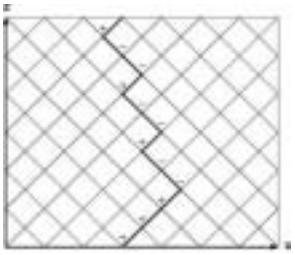

Figure 5.1. The lattice of the $1+1$ dimensional DPRM model of size 14×12. The string is directed in the direction of the z-axis with transverse displacements in the direction of u-axis as we show with the thick zig-zag line.

states with various perturbation strengths: $h = 0, 0.05, 0.1, 0.2, 0.3, 0.4$ for each realisation of random potential;*b)* temperature perturbation: we have used the finite temperature version of the transfer matrix method. The temperature of replica A is set to $T_A = 0.1$. The temperature of replica B is changed as $T_B = T_A + \delta T$ with different temperature shifts $\delta T = 0.1, 0.2, 0.3, 0.4, 0.5, 0.6, 1.2$; *c)* modified Sinai potential: we have looked for the ground states of each replica in the random potentials corresponding to various field strengths $h = 0.01, 0.01, 0.025, 0.05, 0.075$.

2.4.1 Uniform Tilt Field

First we examine the case of the perturbation by a uniform tilt field. In order to simplify the temperature is set to zero $T = 0$. The two replicas have exactly the same random potential. The difference is that replica B is subjected to a uniform tilt field h which amounts to a force acting just on its end,

$$\begin{cases} E_A[V, h_A = 0, u_A] &= \sum_{z=1}^{L} V(u_A(z), z) \\ E_B[V, h_B = h, u_B] &= \sum_{z=1}^{L} [V(u_B(z), z)] - h u_B(L). \end{cases} \tag{5.73}$$

We examine the correlation of the ground-state energies of the perturbed and unperturbed systems through (5.5) evaluated at $T = 0$ so that Φ corresponds to energy fluctuations, $\Phi = E - E_{\rm GS}$.

In Fig. 5.2, the data of the correlation function of the ground-state energies of the perturbed and unperturbed systems and its scaling plot is shown. The data shows a decorrelation of the (free-) energy landscape of the two systems as expected. The scaling plot is obtained using $L_c(h) = h^{-3}$ without any adjustable parameters. The initial part of the master curve is well fitted by the expected form (5.24) using $\alpha = 2/3$, $C_L(F) = 1/(1 + A(L/L_c(h))^{2(\alpha - 1/3)})$ with $A \sim 2.0$, but for $L/L_c(h) \gg 1$ the decay is faster.

2.4.2 Modified Sinai model

In Sec. 2.3 we have proposed a modified Sinai model as an effective model for the free-ends of DPRM under uniform tilt field. Here we numerically study the correlation function of the 'ground-state energies'. The effective Hamiltonian given in (5.71) and

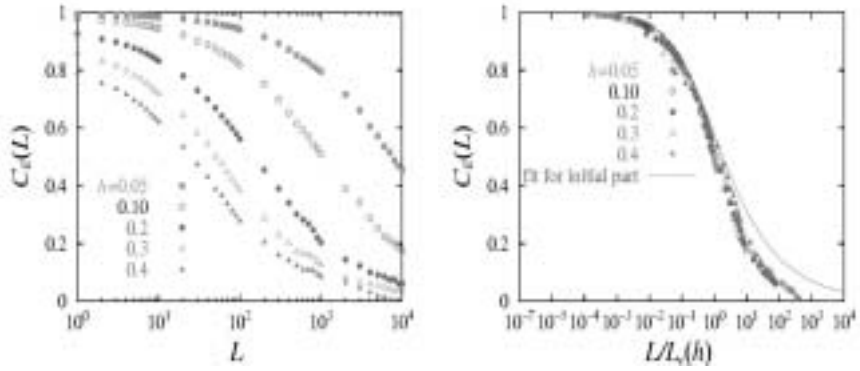

Figure 5.2. $C_E(L)$ of the uniform tilt field case and its scaling plot (*right*) with $L_c(h) = h^{-3}$. The fit is $C_F(L) = 1/(1 + A(L/L_c(h))^{2(2/3-1/3)})$ with $A \sim 2.0$.

(5.72) at a given length L reads as [13] [14],

$$H = H_A + H_B \qquad \begin{cases} H_A &= \frac{1}{2L}x_A^2 + \mathcal{V}(x_A) \\ H_B &= \frac{1}{2L}x_B^2 + \mathcal{V}(x_B) - h\, x_B \end{cases} \tag{5.74}$$

where $\mathcal{V}(x)$ is the modified Sinai potential with correlations,

$$\overline{(\mathcal{V}(x) - \mathcal{V}(y))^2} = u + (u^*(L) - u)\theta(u - u^*(L)) \text{ with } u^*(L) = L^{2/3} \tag{5.75}$$

In first place, we prepare the same *bounded* Sinai potential $V(x)$ for replicas A and B on a 1 dimensional lattice $u = 1, 2, \ldots, R$ of size R by generating random walks confined in a box of size u^*. And for the B replica, we add an extra tilting potential $-hu$.

The correlation function (5.5) of the fluctuation of ground-state energies is computed for various L and h, taking $\Phi = \Delta E(L)$ as the deviation of a ground-state energy from the mean ground-state energy. In Fig. 5.3 we show the correlation function of the fluctuation of the ground state energy as well as its scaling plot using the scaling variable $L/L_c(h)$. In the plot, we have included the master curve of the equivalent DPRM problem shown in Fig 5.2.

It can be seen that the agreement between the modified Sinai model and the original DPRM under uniform tilt field is good. If the original unbounded Sinai potential is used, the agreement becomes very bad for large length scales. Specifically, the correlation function $C_E(L)$ tends to saturate, supporting the picture that RSB is needed to account for the decorrelation of energy landscape of DPRM under uniform tilt field.

[13] Note that here we do not use re-scaled variables such as in (5.67).

[14] The same results are obtained if we consider that the two strings are tilted with $-h$ and $+h$ respectively.

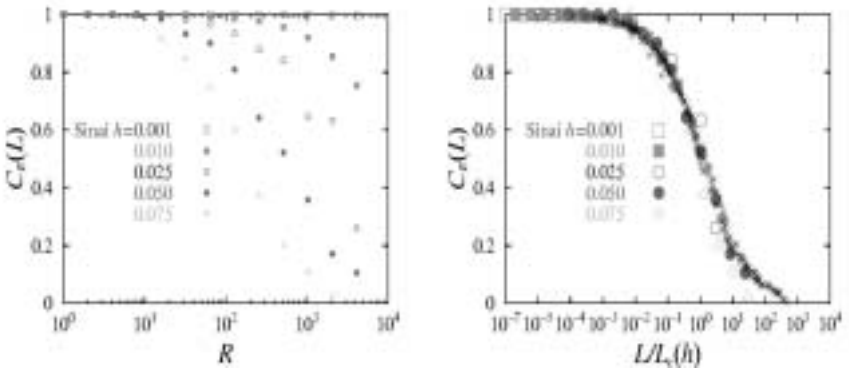

Figure 5.3. $C_E(L)$ of Sinai model under uniform tilt field and its scaling plot (*right*) with $R_c(h) = (0.9h)^{-2}$. In the scaling plot, the master curve of DPRM under uniform tilt field plotted vs $L/L_c(h)$ as in Fig. 5.2 is also included for comparison (black crosses).

2.4.3 Perturbation on temperature

Finally we examine the class of perturbations to which temperature shift belongs (which includes potential change and random tilt field). These perturbations are characterised by the exponent $\alpha = 1/2$ found in Sec. 2.1.2 (which is related to the order of the perturbation $p = 2$ in the replica analysis - see Sec. 2.2.1-).

The Hamiltonians of replicas A and B are exactly the same,

$$E_B[V, u_A] = \sum_{z=1}^{L} V(u_A(z), z)\,; \qquad E_B[V, u_B] = \sum_{z=1}^{L} V(u_B(z), z) \tag{5.76}$$

In Fig. 5.4, the correlation of the ground-state free-energies of the perturbed and unperturbed systems are shown together with its scaling plot. The initial part of the master curve fits nicely into the expected form (5.24) using $\alpha = 1/2$, $C_L(F) = 1/(1 + A(L/L_c(h))^{2(1-1/3)})$ with $A \sim 1.5$. One can see that the decay is faster for $L/L_c(h) \gg 1$.

3. The Random-Energy Exponential model (REEM)

The REM, as introduced by Derrida, is a set of 2^V energy levels that are Gaussian distributed with variance V. This model displays a transition at $T_f = 1/\left(2\sqrt{\ln 2}\right)$ from a PM phase where 2^V energy levels contribute to $\mathcal{Z}$ to a low temperature phase where only a few states are relevant. At low temperatures the system collapses around the very last available state of average energy $E_0 = -V \ln 2$. Here we are interested in the low-T phase so that we will study the random energy exponential model. This model model shares the same low-temperature properties of the REM but has an exponential

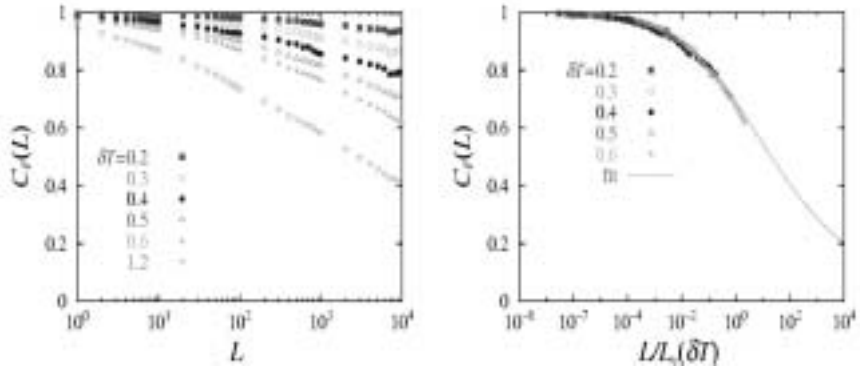

Figure 5.4. $C_F(L)$ of the temperature-shift perturbation case for $T_{\rm A} = 0.1$ and $T_{\rm B} = T_{\rm A} + \delta T$ for various δT. In the right panel we show its scaling plot with $L_c(\delta T) = (0.43\delta T)^{-6}$.

distribution of levels (see Sec. 3.1),

$$P(\epsilon) = \frac{1}{T_f} e^{-\frac{\epsilon}{T_f}} \; ; \qquad \epsilon \in [0, \infty] \tag{5.77}$$

T_f being the transition temperature. Below the transition only levels whose energies are $\epsilon = \mathcal{O}(1)$ contribute significantly to the low-temperature thermodynamics, as expected in a transition driven by an entropy crisis. These transitions have been widely studied because of their connection to the liquid-glass transition [pT87]. The collapse of the number of relevant states is reflexed in the *localisation* of the probability moments ,

$$Y = \sum_i^N \left(\frac{e^{-\beta\epsilon_i}}{\mathcal{Z}} \right)^2 \left\{ \begin{array}{ll} T < T_f & Y = 1 - \mu + \mathcal{O}(\frac{1}{N}) \\ T > T_f & Y = \frac{1}{N} \end{array} \right. \tag{5.78}$$

where $N = 2^V$ is the total number of states and we have introduced the parameter $\mu = T/T_f$. Above the transition *all* the states contribute significantly to the partition function so that Y vanishes as $1/N$, but below T_f the partition function is localised in a few states so that Y becomes a constant .

3.1 Response to a change in temperature

Our aim is to investigate the response of the REM against temperature changes. The general procedure to perform calculations on this model is given in the Appendix E, so that in what follows we discuss the final results obtained for the free-energy and its fluctuations.

In first place, it is useful to consider the free-energy at low temperatures, that reads (E.8),

$$\overline{F} = -T_f \left[\ln N + \gamma(1-\mu) + \ln \Gamma[1-\mu] \right] \quad , \tag{5.79}$$

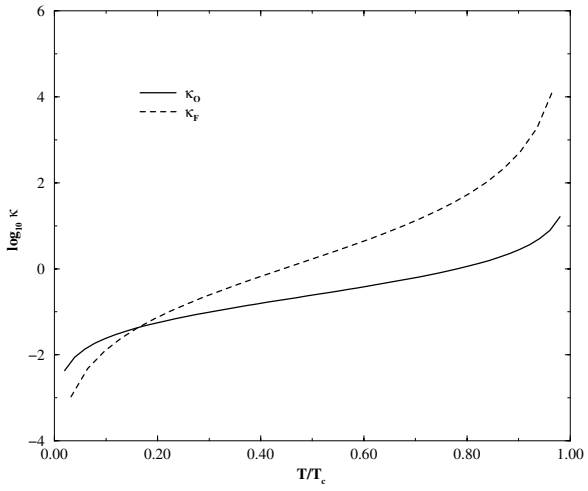

Figure 5.5. Plot of the rejuvenation susceptibilities κ_O (plain line) and κ_F (dotted line) in semi-log scale, as a function of $\mu = T/T_f$. Note that both quantities vanish at $T = 0$ and diverge at $T = T_f$, with different exponents.

where γ is Euler's constant and $\Gamma[x]$ is the usual Gamma function. Note that here the first contribution comes from the fact that the minimum energy that can be drawn from an exponential distribution is $-T_f \ln N$, and thus corresponds to the energy of the ground-state. Fluctuations around the minimum which will contribute to C_F will therefore be of order 1. Since we are at the low-temperature phase we know that entropy fluctuations will also be of $\mathcal{O}(1)$. Therefore in virtue of equation (5.11) we expect that κ_F is a function dependent only on temperature (μ).

In Fig. 5.5 we plot the behaviour in the limit $L \to \infty$ of κ_F versus $\mu = T/T_f$. The susceptibility of the free-energy landscape against temperature changes is given by expression E.12. In the limit $\mu \to 0$ this susceptibility vanishes as $\kappa_F \approx 0.095558\mu^2$ as expected from the fact that only the ground state contributes to the free-energy and the entropy is very small and does not favour the contribution of different states with temperature. Hence one expects the two systems at different temperatures to be strongly correlated. This is precisely the situation met in the Sinai model addresses in the following section where all the low temperature phase is governed by the ground state and the fluctuations around it. Regardless of this, the interesting result is given by the behaviour close to the freezing temperature. Close to $\mu \to 1$ one finds that the susceptibility diverges as,

$$\kappa_F \sim \frac{0.538802}{(1-\mu)^3}. \tag{5.80}$$

This is a signature that close to the "delocalisation transition" the system has a tendency to occupy rather different states. Therefore, even though the model is not chaotic in the sense that the free-energy landscape is fixed at low temperatures, exactly at T_f the model exhibits a strong sensibility to temperature changes and thus is chaotic. We have to point out that close to a critical point chaos can be seen as a critical phenomenon due to the existence of large fluctuations, and no necessarily linked to any specific type of transition [Rit94].

A change in temperature from high to the low temperature phase can lead to significant changes in different observables. Consider an observable $\mathcal{O}_i$ independent of energy such as the position $\mathcal{O}_i = x_i$ in a box of size L. It turns out that this is a random variable whose variance depends on whether we are above or below the transition temperature. Below T_f as there are a few relevant states, it has finite variance so that the mean position is extensive with system size $\langle x \rangle \sim \sqrt{1-\mu}\, L$ [15]. Instead, in the high temperature phase it is sub-extensive $\langle x \rangle \sim L^{\zeta}$ with $\zeta < 1$. Dynamically this implies that a quench from high temperature to $T < T_f$ implies a complete rearrangement of the equilibrium properties which takes place in a slow way.

This is reflected in the response function defined in (5.16) that measures the change of this observable against small temperature changes $\delta = \frac{\Delta T}{T_f}$ within the glassy phase,

$$\mathcal{R}(\delta, \mathcal{O}) = \kappa_{\mathcal{O}} \delta^2 \left(\sum_i \mathcal{O}_i^2 \right) \tag{5.81}$$

The calculation follows similar steps to the computation of C_F. The final result for $\kappa_{\mathcal{O}}$ is is plotted in Fig. 5.5. Its limiting behaviours are the following,

$$\lim \mu \to 0 \quad \kappa_{\mathcal{O}}(\mu) = 1.21497802\ \mu_1 \tag{5.82}$$

$$\lim \mu \to 1 \qquad \kappa_{\mathcal{O}}(\mu) \sim \tfrac{1}{3(1-\mu)}\ . \tag{5.83}$$

Thus, we find that again there is a divergence of the susceptibility close to T_f. Instead, if we compare temperatures above T_f we find that $\kappa_{\mathcal{O}}$ vanishes as $N^{-\alpha(T)}$ with $\alpha(T) < 0$.

The relevance of this result is that a change in temperature implies a big change (extensive with the system size) of the position of the system. In this sense we can conclude that rejuvenation is strong even though the system is not chaotic, because the response of the system to the temperature change is very large. In spite of this, we have to point out that since the states which are available below T_f are finite, the probability to find the system in the same state at T_1 and T_2 is finite in the $N \to \infty$ limit. This probability is related to $\kappa_{\mathcal{O}}$ and reads,

$$P_{12} = \overline{\frac{e^{-\beta_1 e_i}}{\mathcal{Z}(T_1)} \frac{e^{-\beta_2 e_i}}{\mathcal{Z}(T_2)}} = \frac{1}{2}(Y_1 + Y_2) - \kappa_{\mathcal{O}}\ \delta^2 = 1 + \frac{\mu_1 + \mu_2}{2} - \kappa_{\mathcal{O}}\ \delta^2 \tag{5.84}$$

[15] This result can be easily obtained from the squared probability moments in (5.78).

where note that $P_{11} = Y_1$ as it should. Then, it becomes evident that the time-evolution at T_2 would be affected by any previous stay at T_1. To find strong rejuvenation effects in the glassy phase, one needs to generalise the REM or REEM with models such as the generalised or multilevel REM in which there is a hierarchy of phase transitions with different transition temperatures $T_{f,n}$. Still, the results reported in this section give a meaning to the numerical investigations of these more sophisticated models that report very similar effects to those observed experimentally such as rejuvenation and the corrections to perfect memory in temperature shift experiments [SN00, Kaw01, SVDV02].

4. The Sinai Model

The Sinai model belongs to the wide class of random potential models. It can serve as a model of a wide range of systems and in particular of the movement of pinning centres of domain walls [BCGlD90]. Interestingly, the effective potential acting on the end point of the disordered directed polymer in 1+1 dimensions is also of the Sinai type [Méz90, Par90, BO90]. However, as we have seen in Sec. 2, the effective potential itself becomes temperature dependent, and the role of temperature changes in the directed polymer is much more subtle [FH91b, SY02, dSB02].

Here we model the phase space of the pinning centre of a Domain Wall with the Sinai potential. In the following, we consider the discrete version of the Sinai model. The system consists of a box of length L in which we generate a random potential. Each sample of the random potential is constructed as follows, at each site $i \in [1, L]$ we generate a random Gaussian force f_i distributed with zero mean $\overline{f_i} = 0$ and variance $\overline{f_i\, f_j} = \sigma\, \delta_{ij}$. The potential in each site is the sum of the forces in the previous sites $V_i = -\sum_{j=1,i}\ f_j$ and thus is a random walk as a function of the position. Thus correlations (and equivalently barriers) grow like (2.16),

$$\overline{(V_i - V_j)^2} = \sigma\, |i - j| \quad . \tag{5.85}$$

This is always in the low temperature phase, so that the physics in the infinite-volume limit is dominated by the $T = 0$ glassy fixed point [OMM93, CMY98]. From the relation above it is clear that a change in the scale by a factor b is equivalent to a change in energy or $1/T$ of a factor $\sqrt{b}$. As far as the statics are concerned, this means that being at low temperature and having a small system is equivalent to having a larger system at larger temperature. In dynamics however the change in temperature and size implies a change in timescales.

In the following section we analyse exactly the same quantities studied in the REEM, C_F and $\mathcal{R}(\delta, x)$ where we have seen that even if the energy landscape is fixed, the model is extremely sensible to temperature changes around the critical temperature, where the Boltzmann weight 'condensates' into a finite number of sites. Because there is no finite temperature transition in the Sinai model, under a temperature change one only observes mild chaotic effects that are maximum around the crossover temperature $T \sim L^{-1/2}$.

4.1 The effect of temperature changes

The thermodynamics of the Sinai model has been well studied [OMM93, CMY98]. In the large-L limit temperature is irrelevant. The system is frozen or localised in the minima of the potential, so that physical observables are governed by the ground state and its fluctuations. On the one hand, the free-energy grows as $\overline{F} \sim -\sqrt{L}$ independently of temperature and even at small system sizes. The same happens with its fluctuations so that $\overline{\Phi^2} \sim L$ [CMY98]. And, on the other hand, the entropy reaches an L independent value which depends on temperature $\overline{S} = A + 2\ln T$ but its fluctuations around the deepest well are constant $\overline{(\Delta S)^2} = K$ as is shown in Appendix F. Therefore, it is reasonable to expect that in the thermodynamic limit a change in temperature means no significant change in physical observables measuring fluctuations since the ground state properties are temperature independent.

Numerical details: we have generated random potentials generating Gaussian forces with variance $\sigma = 1$ in each site of a box of size $L = 2^k$ with $k = 1, \cdots, 14$. We have averaged over 2000 samples of the random potential for different temperatures or temperature differences in the case of correlations.

In this model corrections to the thermodynamic limit behaviour depend on a single parameter $\ell = \sigma\sqrt{L}/T$. Corrections become important when $\ell \sim 1$ which allows to define at a crossover length scale $L^* \sim (T/\sigma)^2$ between two different regimes:

- $L \ll L^*$: energy barriers are smaller than temperature, so that like in a high temperature phase, all the sites contribute to the partition function .
- $L \gg L^*$: when the system is very large, barriers become too big and the system gets localised, only a few states within the deepest valley contribute significantly to the partition function. The system is effectively at $T = 0$ and its behaviour is governed by the fluctuations around the ground state.

Let us consider for instance *normalised* mean position fluctuations,

$$\overline{\Delta^2} = \overline{\langle x\rangle^2} - \overline{\langle x\rangle}^2 \qquad x_i = \frac{i}{L}\,; \qquad i \in [1, L] \tag{5.86}$$

We expect the following behaviour in the two limiting regimes,

$$\overline{\Delta^2} \begin{cases} \frac{1}{120}\ell^2 + \mathcal{O}(\ell^4) & \ell \ll 1 \\ \frac{1}{12} + \mathcal{O}\left(\frac{1}{\ell^2}\right) & \ell \gg 1 \end{cases} \tag{5.87}$$

The small ℓ behaviour is obtained by a high temperature expansion. For large ℓ, average position fluctuations should approach the position fluctuations of the ground state. We expect that since the probability distribution of the position of the ground state is uniform, $\mathcal{P}(x^*) \sim 1/L$ the average fluctuations of the ground state position are $\overline{\Delta^{*2}} = 1/12$. This last result is equivalent to that found in the REEM where in the low temperature phase

the average position is a random variable with finite variance. However, we will see that when comparing two systems at different temperatures the susceptibility is not constant as in the REEM but vanishes for large system sizes.

In Fig. 5.6 we show the results for different temperatures versus the scaling variable $\ell = \sigma\beta\sqrt{L}$. As we can see in the figure, the behaviour for small ℓ matches nicely with the expected $\ell^2/120$. For large l note that the scaling function for $\overline{\Delta^2}$ approaches the $1/12$ expected for the average fluctuations of the position of the absolute minimum. Numerically the crossover takes place at $\ell \simeq 3$, hence we can estimate that $L^* \simeq 10\, T^2$. This

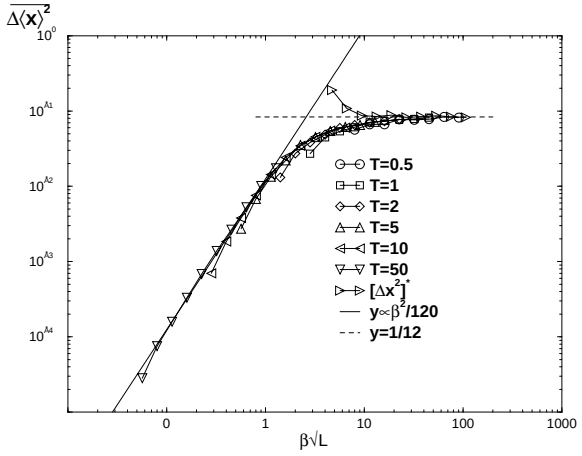

Figure 5.6. Sinai Potential: $\overline{\Delta^2}$ plotted versus the scaling variable $\ell = \beta\sqrt{L}$ for $T = 1,\ 2,\ 10,\ 50$ and 100. The dashed line corresponds to the position fluctuations at zero temperature. For small l we have plotted a line showing the power-law behaviour $\frac{1}{120}\,\ell^2$.

static crossover is exactly mapped to the dynamical crossover from a Brownian diffusive regime to an activated regime as we will see in the analysis of the correlation length in Sec. 5.1.

In the large ℓ limit, regardless of temperature the physics is dominated by the ground state, hence we expect that systems at different temperatures are correlated in this limit. From the analysis of two temperature quantities, we arrive to the conclusion that there is also a crossover length scale (L^*) which separates the high-T phase from the $T = 0$ phase but that depends on the observable. Nevertheless, when the temperature difference is infinitesimally small, all the crossover length scales coincide with the crossover length obtained for the single temperature quantities: $L^* \sim T^2$.

4.1.1 Free-energy correlation functions

As we can see in the inset in Fig. 5.7 free-energy correlations are a non-monotonous function of L. For small L the systems at different temperatures start decorrelating but at a certain length, $L^*(T_1, T_2)$, C_F reaches a minimum. Then, it starts increasing to eventually reach 1 when $L \to \infty$ regardless of the temperature difference (provided it is finite) as expected.
We can thus distinguish between two different regimes in the behaviour of C_F,

- $L < L_F^*$
  For small system sizes at large enough temperatures there are no significant barriers so that all the sites contribute to $\mathcal{Z}$. A high temperature expansion reveals that in this limit entropy is extensive $S \sim L/T$, so that entropy fluctuations $\Delta S \sim L^2$ are much larger than free-energy fluctuations $\Phi \sim \sqrt{L}$. Therefore we expect the two systems to decorrelate. Actually a high temperature expansion yields the following expression for the correlation function reads,

$$1 - C_F \ \propto \ (\beta_1 - \beta_2)^2 \ L \qquad (\Delta\beta\sigma\sqrt{L} \to 0), \tag{5.88}$$

  note that for small temperature changes $\Delta\beta\sigma\sqrt{L} = \delta^2 \, \ell^2$ so that following eq. (5.11) we can express κ_F in terms of the adimensional parameter $\ell \equiv \sigma\sqrt{L}/T \to \kappa_F \sim \frac{\sigma^2 L}{T^2} = \ell^2$.

- $L \gg L_F^*$
  In this limit the system is governed by the ground state and its fluctuations, thus when $L \to \infty$ the free-energy landscape is independent of temperatures and $C_F = 1$. In the Sinai model, we know that in the low T/large L limit, on average, entropy ($\sim \ln T$) is much smaller than free-energy ($\sim \sqrt{L}$). More specifically, free-energy fluctuations $\overline{\Phi^2} \sim L$ are much larger than entropy fluctuations that are constant (see Appendix F). Thereby, we expect for small δ the following behaviour for the susceptibility κ_F,

$$\lim_{L\to\infty} \ \kappa_F \longrightarrow \ \frac{K \, T^2}{\sigma^2 L} = \frac{K}{\ell} \ \ (\delta T \to 0) \ . \tag{5.89}$$

  Note that in this limit it is as well a function of the reduced variable ℓ that vanishes for $\ell \to \infty$, this is to say in the limits $L \to \infty$ or $T \to 0$ which are equivalent.

- Crossover
  The crossover between both regimes will take place at a certain length L_F^* such that $\Delta\beta\sigma\sqrt{L_F^*} \sim \Delta T/\sigma\sqrt{L_F^*}$, which yields $L_F^* \sim T_1 T_2/\sigma^2$. The maximum of $1 - C_F$ actually occurs at $L_F^* \approx 10 \ T_1 T_2/\sigma^2$ (see left panel in Fig. 5.7).

  For small δT we have seen that κ_f is a scaling function depending on a single parameter ℓ and that the crossover between the two limiting regimes takes place when $\ell \sim \ 10$, precisely at the point where decorrelation is maximal. As a matter of fact, the crossover coincides with the crossover already observed for thermodynamic quantities at a fixed

temperature and takes place at $L^* \approx 10\ T^2$. Therefore, κ_F is a scaling function of the variable $\ell = L/L^*$ with the following limiting behaviours,

$$f(\ell) \begin{cases} \sim \ell & \ell \to 0 \\ \sim \frac{1}{\ell} & \ell \to \infty \end{cases} . \tag{5.90}$$

In Fig. 5.7 we plot κ_F versus the scaling variable $\frac{L}{L^*}$ for different temperature differences. As expected the maxima of all the curves lie on the same value of $\frac{L}{L_F^*}$. However, as we show in the left plot of Fig. 5.7, this scaling only works when temperature differences are not too big as one would expect.

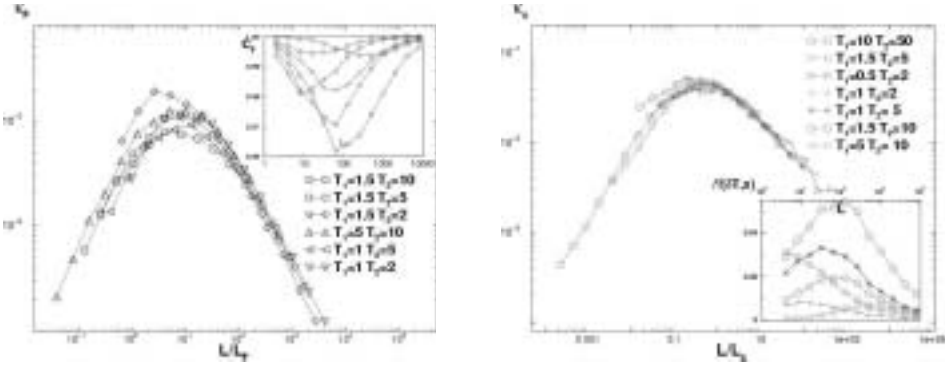

Figure 5.7. Susceptibilities. *Left:* κ_f as a function of $\frac{L}{L_F^*}$ for different pairs of temperatures (T_1, T_2). Note that curves with big temperature differences do not scale. In the inset we show C_F versus system size for various temperature differences. *Right:* κ_x plotted versus L/L_x^* for different T_1 and T_2. In the inset we show $\mathcal{R}(\delta T, x)$ versus system size for different temperature differences.

4.1.2 $\mathcal{R}(\delta T, x)$: position differences

In Fig. 5.7 we show the results for the average distance shift $\mathcal{R}(\delta T, x)$ as defined in (5.16) where $\mathcal{O}_i = x_i = i/L$, $i \in [1, L]$, for several temperature differences. Even though we have seen that there is no true chaos it is still interesting to study if the response to temperature changes might lead to rejuvenation effects in dynamical measurements.

As we can see in the inset of Fig. 5.7, $\mathcal{R}(\delta T, x)$ is non-monotonic with L and follows a behaviour rather parallel to that found for $1 - C_F$. The crossover length scale L_x^* determines the same well defined regimes:

- $L \ll L_x^*$
  For high temperatures, the system decorrelates because all the sites contribute to the correlation function an therefore $\mathcal{R}(\delta T, x)$ (and correspondingly κ_x) increases with L. This situation is analogous to that found for κ_F, where a high temperature expansion was enough to recover numerical results. As shown in Appendix G, we find that in

this regime $\mathcal{R}(\delta T, x) \approx \frac{1}{120}(\Delta\beta)^2\sigma^2 L$ and thus, for small temperature changes the susceptibility defined in (5.17) depends only on ℓ: $\kappa_x \sim \ell^2$.

- $L \gg L_x^*$

  The behaviour at large L should be governed by ground state fluctuations. Starting from (5.17) we note that it is not enough to consider the ground state and its surrounding sites because these yield contributions to $\langle x\rangle$ which are $\mathcal{O}(1/L)$, and, hence, much smaller than those arising from the valley closest in energy [16]. Typically the distance between the absolute minimum and the minimum of this valley is of $E = \eta\sigma\sqrt{L}$ in energy and of $D = x - x^* = \mathcal{O}(1)$ in position space. Thereby we can approximate the partition function by , $\mathcal{Z} = e^{-\beta V^*}(1 + e^{-\beta\eta\sqrt{L}})$ to evaluate thermal averages. Consequently, at leading order in $e^{-\beta\eta\sqrt{L}}$ we get for the main term entering in the computation of κ_x (5.17),

$$\langle V_x\, x\rangle - \langle x\rangle\langle V_x\rangle \;\approx\; \mathrm{D}\,\eta\,\sqrt{L}\,e^{-\beta\eta\sqrt{L}}\ . \tag{5.91}$$

  The average of the square power of this expression depends on the probability distribution of the excitations $P(\eta, \mathrm{D})$. In general, we do not expect any correlation between valley-to-valley distance and energy gaps [17] so that, we can assume that the probability distribution factorises $P(\eta, \mathrm{D}) = h(\eta)\ p(\mathrm{D})$. In the limit $L \to \infty$ we have that the average of (5.91) reads,

$$\begin{aligned}\overline{\mathrm{D}^2 e^{-2\beta\eta\sqrt{L}}(\eta\sqrt{L})^2} \;&=\; \int_0^\infty d\eta\, h(\eta) e^{-2\beta\eta\sqrt{L}}(\epsilon\sqrt{L})^2 \\ &\overset{\beta\sqrt{L}\to\infty}{\sim}\; \frac{h(0)}{(\sigma\beta)^3\sqrt{L}}\end{aligned} \tag{5.92}$$

  which yields [18],

$$\kappa_x \sim \frac{1}{\sigma\beta\sqrt{L}} \quad \lim\left(\sigma\beta\sqrt{L}\right) \to \infty\ . \tag{5.93}$$

- Crossover
  As for the free-energy correlation, we can extract a crossover length scale which separates both regimes. The crossover length that is obtained is $L_x^* \sim (T_1\ T_2)^{\frac{4}{3}} T^{-\frac{2}{3}}$, that coincides with L_F^* in the limit $T_1 = T_2$.

[16] Note that we work with normalised positions in the range $[1/L, 1]$.

[17] This assumption has been numerically checked.

[18] This result holds provided $h(0) \sim B \neq 0$. The fact that the constant that not depend on L is guaranteed from the normalisation condition for the distribution of energy cost of the excitation $\mathcal{H}(\Delta E)$. Since on average $\Delta E \sim \sqrt{L}$, normalisation yields $\mathcal{H}(\Delta E)\sqrt{L} = h(\epsilon = \Delta E/\sqrt{L})$. Therefore $g(0)$ is either a constant or zero, but, numerically, it is easy to check that $h(0) \neq 0$.

For small temperature changes $\kappa_x = \frac{1}{\delta^2}\mathcal{R}(\delta T, x)/\overline{\Delta^{*2}}$ is, as well as, κ_F a scaling function of the variable $\ell = \sigma\beta\sqrt{L}$. Nevertheless, we find that the limiting behaviours are different to those of κ_F,

$$\kappa_x \begin{cases} \sim \ell^2 + \mathcal{O}(\ell^4) & \ell \ll 1 \\ \sim \frac{1}{\sqrt{\ell}} + \mathcal{O}\left(\frac{1}{\ell}\right) & \ell \gg 1 \end{cases} \tag{5.94}$$

This reflects the fact that that the two observables probe different mechanisms. In the right panel of Fig. 5.7 we show the scaling plot for different pairs (T_1, T_2). Note that *all* the curves display the maximum at the same value of the scaling variable $\frac{L}{L_x^*} \simeq 10$.

4.1.3 Discussion: The Sinai Model the DPRM and the REEM

The outcome of the numerical analysis of the Sinai potential is clear: in the thermodynamic limit statistical properties are governed by the $T = 0$ fixed point. This means that regardless of temperature, for large enough system sizes, the system only sees the free-energy valley associated to the minimum. Effectively this situation is equivalent to say that, in this limit, there is no chaos in temperature since the statistical properties are those of the minimum of the potential.

We have seen in the REEM that the existence of a transition from a high temperature phase to a localised phase where all the states are very close in energy can enhance a large response against temperature changes.

However, this situation is very different from that what happens in the directed polymer problem discussed in Sec. 2. Even though this model has no thermodynamic transition either, it is extremely sensible to an external perturbation which leads to the decorrelation of systems at different temperatures. This is due to existence of anomalous large excitations which have a very low free-energy cost $\sim L^{1/3}$. These excitations cost a lot of energy $\sqrt{\overline{\Delta E^2}} \sim L^{1/2}$ but are very favoured entropically $T\sqrt{\overline{\Delta S^2}} \sim L^{1/2}$, so that these two contributions cancel to yield a low cost in free-energy. In the Sinai model these anomalous excitations do not exist because entropy is too small (not extensive) to cancel its energy cost ($\sim L^{1/2}$).

We have already pointed out that different observables probe different mechanisms, leading to different crossover length scales (L_x^* and L_F^*) which are equivalent to $L_T^* \sim T^2$ in the limit of vanishingly small temperature differences. Nonetheless, the important point here is that the maximal decorrelation length and the crossover length scale at each temperature are related as follows: $L_{T_1}^* < L_{x/F}^* < L_{T_2}^*$. This implies that for small system sizes $L < L_1^*, L_2^*$, both systems decorrelate as expected in a random high-temperature phase. The maximum decorrelation takes place at system sizes $L = L_{x,F}^*$ when the system at T_1 is already localised whereas the system at T_2 is still delocalised. The strong influence of temperature shifts in this case is a smeared out version of the infinite susceptibility found in the REEM, in which there is a true finite-temperature phase transition, and not a mere crossover as in the Sinai case. However, when we increase the

system size when $L_1^* < L_2^* < L$ both systems are governed by the zero temperature fixed point and therefore, correlations increase.

5. Rejuvenation in the absence of chaos: dynamics of the Sinai model

The aim of this section is to study the temperature cycling experiments which are carried out in spin glasses that have shown striking rejuvenation and memory effects [Bou00, BDHV01]. Our main goal here is see to what extent these effects are already present in the Sinai model which is hierarchical by construction. We have performed numerically the standard temperature cycling experiment: quench from infinite temperature down to T_1 and let the system relax during t_{w_1}; then change the temperature to $T_2 = T_1 + \Delta T$ and let the system evolve during t_{w_2} and finally go back to T_1. We have studied cycles with positive and negative ΔT for several waiting times and frequencies.

The dynamics of this model have been well studied, both analytically [BCGlD90, DMF99] and numerically [LD98]. Single-time as well as two-time quantities have been analysed. Here, we shall study one observable of both types. First we analyse the correlation length as well as its ageing properties and then we define an 'a.c. susceptibility' that should be closely related to the analogous observable studied in spin-glasses.

Numerical details: in the simulations we have used boxes of length $L = 1024$ with periodic boundary conditions. The dynamics has been simulated by the Monte Carlo method using Metropolis algorithm. For each realisation of the random potential (with $\sigma = 1$), in order to sample adequately the energy landscape we have considered all possible initial conditions ($L = 1024$) and we have averaged over $n \sim 100$ different histories for each starting point. The total number of samples used in temperature cycling experiments is around $200 - 300$.

5.1 Correlation length

We have analysed the correlation or explored length defined as follows,

$$\xi^2(t) = \overline{\langle (x(t) - x(0))^2 \rangle}. \tag{5.95}$$

The brackets and overline mean that we average over both the $L \times n$ histories and samples respectively. The initial condition is a uniform distribution equivalent to a quench from infinite temperatures. The interest of studying this quantity is that it gives information about the *large scale* mechanisms and thus about the global ageing process.

The time evolution for the correlation length at different temperatures is shown in Fig. 5.8. The growth of the correlation length depends exclusively on a temperature dependent microscopic timescale $\tau_0(T)$. This timescale is related to the crossover between two different dynamical regimes [BCGlD90, DMF99]:

- $t \ll \tau_0$: Short time dynamics where no barriers are present, so that in this regime we have usual Brownian diffusion $\xi^2(t) = D\,t$.

- $t \gg \tau_0$: Long time, activated dynamics, with an activation time which follows an Arrhenius law, $t = \tau_0 \exp[B/T]$, with a typical barrier $B \sim \sigma\sqrt{L}$ [BCGlD90], leading to $\xi^2(t) \sim (T/\sigma)^4 \ln^4(\frac{t}{\tau_0})$.

The crossover takes place when barriers become comparable to temperature so that activation between valleys dominates the dynamics. This crossover is directly related to the static crossover found for position or free-energy correlations from a high-temperature regime (no barriers) to a (thermodynamic) low-temperature regime (see Sec. 3.47). The microscopic timescale can be thus identified with the typical time that the system takes to explore this static crossover length scale $L^* \simeq 100\ (T/\sigma)^2$. Therefore, for $\sigma = 1$, $\tau_0(T) = L^{*2}/D \simeq 200\ T^4$, ($D$ can be evaluated numerically by measuring ξ^2 -see Fig. 5.8-. We find $D \approx 0.5$).

From the previous discussion we expect that the correlation length at a given temper-

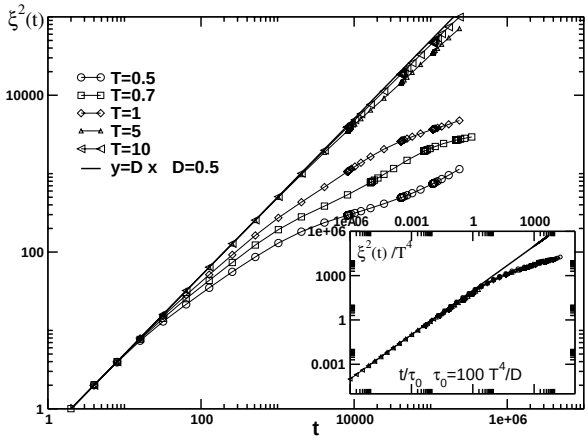

Figure 5.8. Correlation length versus time for different temperatures. The solid line corresponds to the short time diffusive behaviour $\xi(t) \sim \sqrt{t}$. In the inset we plot ξ^2/T^4 versus the scaling variable $\tau = t/200\ T^4$. Averages over 75×1024 histories.

ature (5.95) can be expressed in terms of the rescaled times $\tau = t/\tau_0(T)$ as follows $\xi^2 = T^4 f(\tau)$, where $f(\tau)$ has the following limiting behaviours,

$$\begin{cases} \tau \ll 1 & f(\tau) \sim \tau \\ \tau \gg 1 & f(\tau) \sim \ln^4 \tau \end{cases} \tag{5.96}$$

This scaling behaviour works very well, as shown in the inset of Fig. 5.8, where we rescale together all temperatures. This situation is analogous to that depicted for domain wall dynamics in the droplet approach to spin glasses outlined in Sec. 2.3. The growth of equilibrium domains at long times becomes activated over barriers which grow with the size ℓ of the excitations as $B(\ell) = \Upsilon(T)\ell^\psi$, where $\Upsilon(T)$ is a function of temperature. This leads naturally to a logarithmic growth of the size of the droplets, $\ell \sim (\ln[t/\tau_0])^{1/\psi}$,

where τ_0 is a microscopic attempt time [19] [BDHV01, DVB$^+$01, JYN$^+$02b]. The Sinai case corresponds to $\psi = 1/2$ and $\tau_0 \propto \ell^2$, thus the correlation length is the analogous of the domain size in the droplet description.

In order to characterise the ageing process we e correlation length we have studied the dependence on t_w and t of the following quantity $\Xi(t, t_w) = \xi^2(t + t_w)/\xi^2(t_w) - 1$. From (5.96) we distinguish three different regimes,

$$\Xi(t, t_w) \begin{cases} \text{a)} & t/t_w & t_w, t \ll \tau_0 \\ \text{b)} & \ln\left(\frac{t+t_w}{t_w}\right) / \ln\frac{t_w}{\tau_0} & t_w \gg \tau_0 \; t \ll t_w \\ \text{c)} & \ln\left(\frac{t}{t_w}\right) / \ln\frac{t_w}{\tau_0} \left(\ln\frac{t}{\tau_0} / \ln\frac{t_w}{\tau_0}\right)^3 & t_w \gg \tau_0 \; t \gg t_w \end{cases} . \tag{5.97}$$

Different regimes can be reached changing temperature and waiting time. In Fig. 5.9 we plot $\Xi(t, t_w)$ versus the adequate scaling variable for regimes a) and b). Note the numerical results reproduce the analytical predictions. Remarkably we have been able to scale curves for different temperatures. Regime a) does not need to take into account any microscopic time τ_0. But, on the contrary, in regime b) τ_0 enters in the scaling variable and note that we have been able to superpose all the curves using $\tau_0 \sim T^4$. Actually,

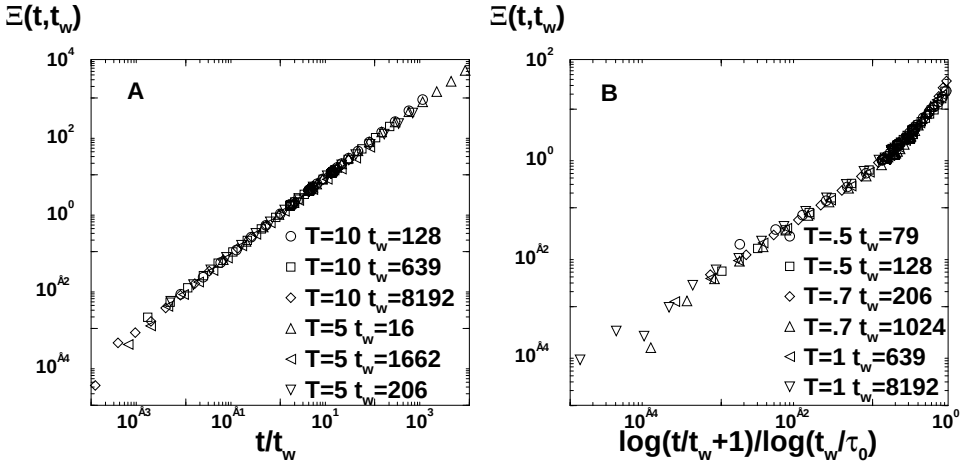

Figure 5.9. Ageing in the correlation length. We plot $\Xi(t, t_w)$ in the regimes a) and b) as expressed in (5.97). *Regime a)* ageing when $t, t_w \ll \tau^* \; T^4$. We plot $\Xi(t, t_w)$ versus the scaling variable t/t_w for temperatures $T = 5$ and 10 for different waiting times. *Regime b)* ageing when $t_w \gg T^4 \; \tau^*, \; t \simeq t_w$. We plot $\Xi(t, t_w)$ versus the scaling variable $\ln(\frac{t+t_w}{t_w}) / \ln(\frac{t_w}{\tau_0})$ for temperatures $T = .5, \; .7$ and 1 for different waiting times.

we find that since this is a purely activated model, the scaling variable for long times is

[19] In the most general case, τ_0 is renormalised by critical fluctuations if the system is close to the critical point .

logarithmic. Such scaling is found experimentally in coarsening systems rather than in spin glasses. We have to note that barriers in this model do not depend on temperature and, therefore, we should expect cooling rate effects to be present. But still, this situation reflects that dynamics at different length scales are exponentially separated in this model and we expect it to account for the mild rejuvenation phenomena observed also in random ferromagnets [Bou00, HVD$^+$00].

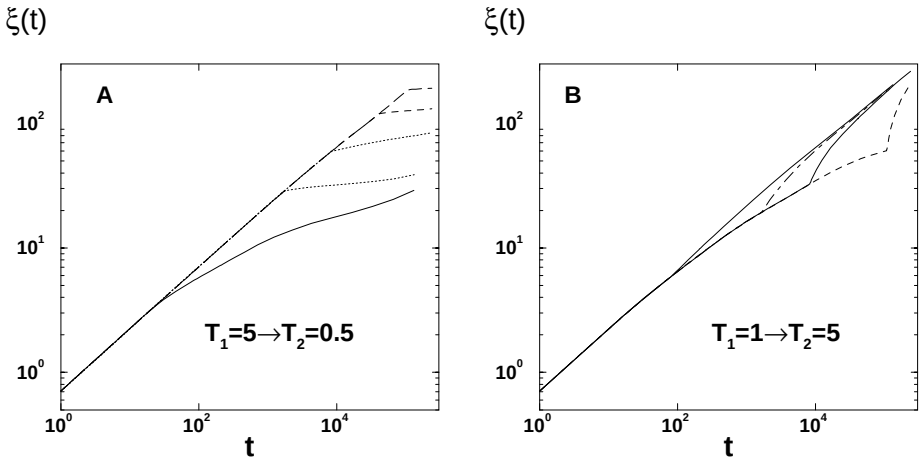

Figure 5.10. Correlation length $\xi(t_w)$ versus time for the following experiments: *Left*) spend t_w at $T_1 = 5$ and then quench the system down to $T_2 = .5$ for $t_w = 16,\ 1662,\ 8192,\ 40959$ and 106494 from bottom to top; *Right*) spend t_w at $T_1 = 1$ and then heat the system up to $T_2 = 5$ for $t_w = 79,\ 1662,\ 8192$ and 106494.

So far we have seen that ξ is a monotonic function of time and temperature. The temperature only plays the role of slowing down dynamics, therefore a change in temperature only changes the growth law. Any time t_w spent at a temperature T_1 is equivalent to having spent an effective time $t_{\rm eff}(t_w, T_1, T_2)$ at T_2 such that $\xi^2(t_w, T_1) = \xi^2(t_{\rm eff}, T_2)$. Thus in temperature cycling protocols there is no trace of the chaotic effects observed experimentally on the correlation length itself (see Fig. 5.10). This is presumably due to the fact that, in a.c. experiments, after a negative temperature shift one probably observes how the 'domain walls' reconform on a scale which is small compared to $\xi(t_w)$. This can be studied by defining a suitable *a.c. susceptibility* that probes these 'small' length scales and might show an interesting behaviour during temperature cycling, not revealed by $\xi(t_w)$ (see Fig. 5.10).

5.2 Susceptibility

In order to probe *smaller* length scales that are more sensitive to temperature changes, we have defined the following a.c. susceptibility $\chi(\omega, t_w)$ [20]:

$$\chi(\omega, t_w) \equiv \overline{\left\langle \left(x(t_w + \frac{1}{\omega}) - x(t_w) \right)^2 \right\rangle \Big|_{\mathcal{P}(x,t_w)}} \quad , \tag{5.98}$$

where the average is taken over the probability $\mathcal{P}(x, t_w)$ that a particle is at position x at time t_w, with a uniform distribution of particles at time $t = 0$ [21]. In other words, we measure the typical extra distance travelled by particles during a time $1/\omega$, weighted by the dynamical distribution at time t_w. The study of this 'response' function is useful because the results admit an intuitive interpretation in terms of the evolution of $\mathcal{P}(x, t_w)$, which is the quantity that keeps track of the thermal history of the system.

In order to compare with experiments, one should be in the following conditions: long waiting times t_w and low frequencies ω (as compared to microscopic timescales), but such that $\omega\ t_w \gg 1$. This last condition is imposed by the fact that a harmonic response can only be measured on a time larger than one oscillation period. This also ensures that one is in a regime where the FDT violations are weak and one can identify the fluctuation that we measure to a *response* (see Sec. 2.4.1).

From the results of the simulations we observe that the effect of ageing at temperature T_1 on the relaxation at T_2 depends strongly on the temperature difference and on the waiting time. This effect can be quantified by defining an effective time. For instance, when cooling the system from T_1 to T_2 one expects that if the system is completely rejuvenated, the relaxation curve $\chi_{T_1,T_2}(\omega, t_{w2})$ should correspond to that obtained after quenching from high temperature $\chi_{\infty,T_2}(\omega, t_{w2})$. (Here t_{w2} is counted from the time at which the system reaches T_2). However, if the relaxation at T_1 affects ageing at T_2 then rejuvenation is only partial and the new relaxation corresponds to that of the system after ageing during an effective time $t_{\rm eff}$ at T_2, $\chi_{\infty,T_2}(\omega, t_{w2} + t_{\rm eff})$. Thus if $t_{\rm eff} = 0$, rejuvenation is complete. In Fig. 5.12 we show how this effective time is measured. Note that only the late part of the curves can be superimposed: there is a transient that cannot be accounted for using an effective time. A similar effect can be observed in spin-glasses. The same effective time can also be defined when heating back the system, as a measure of memory recovery.

In the Introduction (Sec. 1.3.2) we have already described the experimental observations so that we will directly comment the outcome of simulations.

- Rejuvenation in negative ΔT shifts.
  In Fig. 5.13 we plot two different examples of cycles with negative shifts in temperature: plot A corresponds to the cycle $T_1 = 5$, $T_2 = 0.5$ and plot B to $T_1 = 2$,

[20] Such a quantity was also considered in [LD98, DMF99].
[21] We have also investigated the case where the initial distribution is localised on an arbitrary point, with similar results.

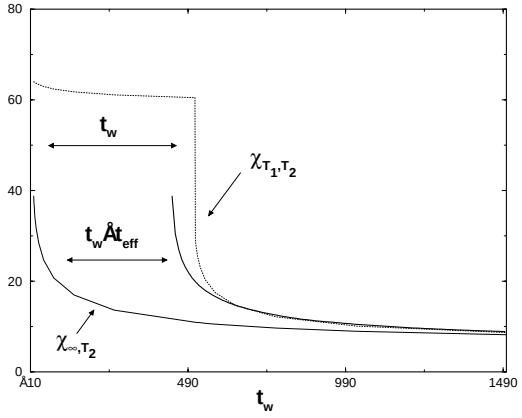

Figure 5.11. Measure of the effective time when cooling the system down to $T_2 = 0.5$ after having spent $t_{w1} = 512$ at $T_1 = 5$ at $\omega = 1/128$. Note that only the late part of the curves can be superimposed: there is a transient that cannot be accounted for using an effective time.

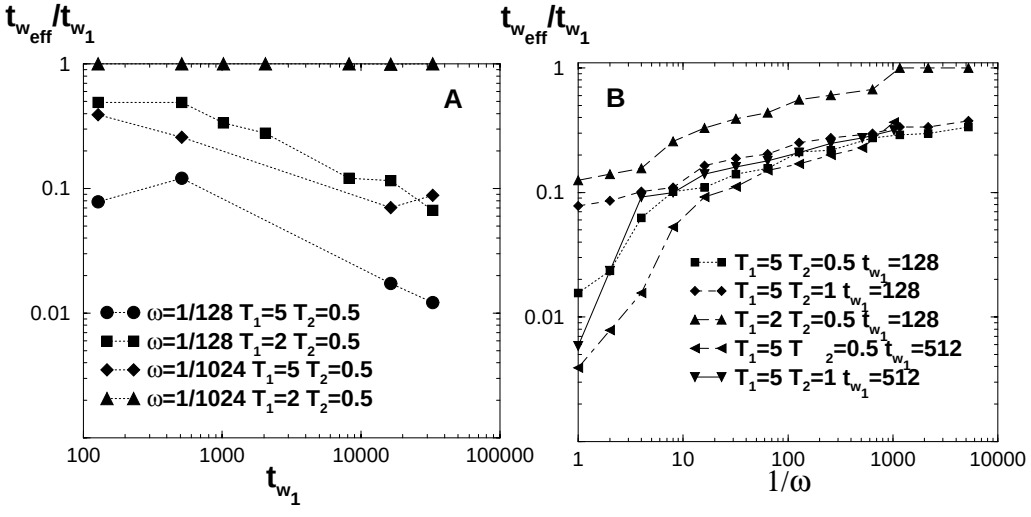

Figure 5.12. Normalised effective times $t_{\rm eff}/t_{w1}$ corresponding to negative temperature shifts: plot A) at fixed ω versus t_{w1}, plot B) at fixed t_{w1} versus $1/\omega$.

$T_2 = 0.5$. The main observation here is that there is clear rejuvenation, with an effective shift time that decreases as ΔT increases, as in the experiments. Intuitively, this corresponds to the fact that since the potential is self-similar, the *local* dynamics probed by $\chi(\omega, t_w)$ is not sensitive to the depth of the potential valley that is currently occupied. Therefore, ageing at T_1 has already selected some low-lying valleys, but the

intra-valley dynamics is insensitive to this. This is precisely the underlying idea in the approach based on a hierarchical energy landscape [BDHV01]. Lower frequencies, that correspond to larger length scales, are less easily rejuvenated, as expected, since the separation of time scales is not as sharp. This is measured quantitatively with the (normalised) effective waiting times that are plotted in Fig. 5.12 as a function of both t_{w1} and $1/\omega$.

- Memory after heating in negative ΔT shifts.
  On heating the system back to the initial temperature T_1, some memory is observed. However, when the temperature difference is not very large, some effective time, accounting for the period spent at T_2, must be included, as in the experiments, and a strong transient 'memory anomaly' is observed, even for quite large ΔT's (see plots A and B in Fig. 5.13). This memory anomaly is defined as,

$$\Delta\chi = \chi(t_{w1} + t_{w2} + 1/\omega) - \chi(t_{w1}^-) \ , \tag{5.99}$$

  where $\chi(t_w = t_{w1}^-)$ is the susceptibility just before the quench and $\chi(t_{w1}+t_{w2}+1/\omega)$ corresponds to the first possible measurement at frequency ω after heating back to T_1. The dependence of the memory anomaly on frequency and waiting time is shown in figures 5.14 and 5.15. In Fig. 5.14 we show how the memory anomaly corresponding to the cycle with larger ΔT ($T_1 = 5,\ T_2 = .1$) varies with the time t_{w2} spent at T_2, at fixed $\omega = 1/128$ and $t_{w1} = 1024$. From the inset, $|\Delta\chi|$ decreases with increasing ΔT, as expected when temperature enhances the separation between length scales. Note that we have always observed this memory anomaly to be negative, *i.e.* the reference curve is always reached from below. On the plot in Fig. 5.15 we show how the memory anomaly depends on the frequency ω. Since the susceptibility at t_{w1} itself depends on ω we plot the relative variation of the susceptibility with respect to $\chi(t_{w1}^-)$ at fixed $t_{w1} = t_{w2} = 1024$. In the inset we show $\Delta\chi/\chi(t_{w1}^-)$ versus ω. Note that $\Delta\chi/\chi(t_{w1}^-)$ is always negative and decreases in absolute value with increasing $1/\omega$. This same effect has been investigated in the REM in [SVDV02] by Sasaki et al. to find that the anomaly can be both positive and negative when one works in the vicinity of a transition temperature. In the Sinai model we have not been able to observe such a positive anomaly. For smaller ΔT's these effects are blurred because length scale separation becomes weak. Ageing at different temperatures is cumulative and $\Delta\chi/\chi$ is also larger (see fig 5.13 for the $T_1 = 2 \to T_2 = 0.5$ cycle). For these smaller ΔT's, we have found that the memory anomaly becomes non monotonous with frequency.

- Positive temperature cycles.
  For positive ΔT we have also observed that the third stage is completely independent of t_{w1}. Heating back the system to T_2 erases the initial ageing accumulated at T_1. This is expected, since the dynamics at T_2 allows the system to leave the traps that it had slowly explored at T_1. The new relaxation at T_1 is aged, but the age is only due to the effect of ageing at T_2. This is similar to the effect observed experimentally.

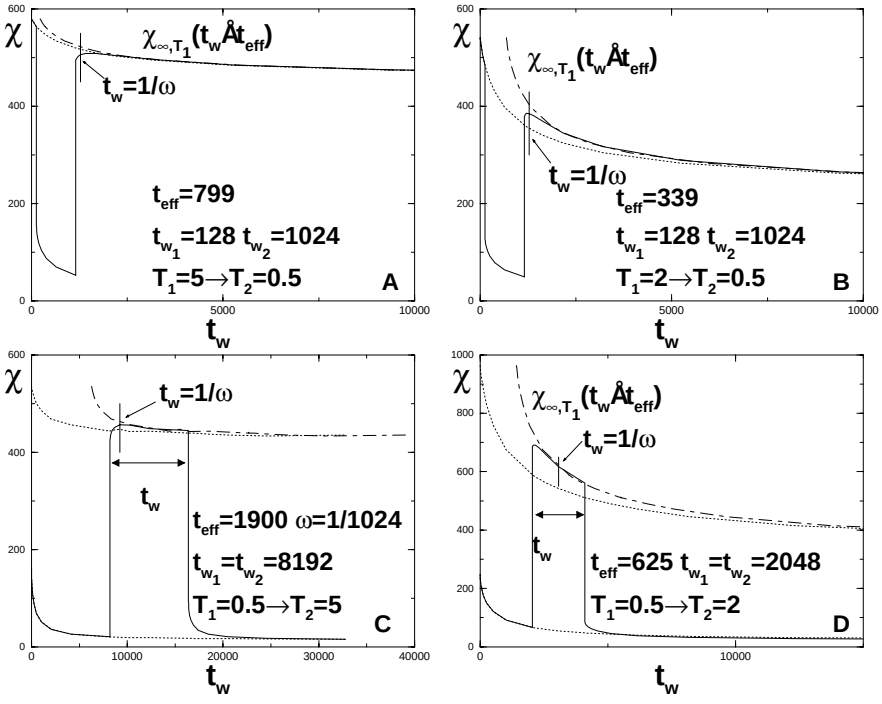

Figure 5.13. Negative and positive temperature cycles. Plots A and B correspond to cycles with $\Delta T < 0$, for fixed frequencies and waiting times, $\omega = 1/128$, $t_{w_1} = 128$ and $t_{w_2} = 1024$; cycle A) $T_1 = 5$, $T_2 = 0.5$ and cycle B) $T_1 = 2$, $T_2 = 0.5$. Plots C and D correspond to cycles with $\Delta T > 0$; for cycle C) $T_1 = 0.5$, $T_2 = 5$, $\omega = 1/1024$ and $t_{w_1} = t_{w2} = 8192$ and for cycle D) $T_1 = 0.5$, $T_2 = 2$, $\omega = 1/1024$ and $t_{w_1} = t_{w2} = 2048$.The solid vertical lines in each plot correspond to the first possible measurement in an experiment at frequency ω which is $t = 1/\omega$.

In the study of temperature chaos in the previous section we have seen that in the large size limit this model is effectively at zero temperature, so that temperature shifts are not interesting in this limit. Nevertheless, for finite sizes/finite times, some interesting crossover phenomena qualitatively reproduce the spin-glass phenomenology. In particular, dynamical rejuvenation effects in the absence of temperature chaos are observed. This rejuvenation is ascribed to the local dynamics, which, since the potential is self-similar, is insensitive to the particular valley that has been reached during ageing at a higher temperature. Still, the separation of timescales/length scales with temperature is much weaker that in experimental spin glasses [BDHV01], partly due to the rather modest time scales investigated in the present study. Correspondingly, abrupt rejuvenation as the temperature is decreased and strict memory when the temperature is cycled cannot be achieved. Rejuvenation and memory are present *in embryo*.

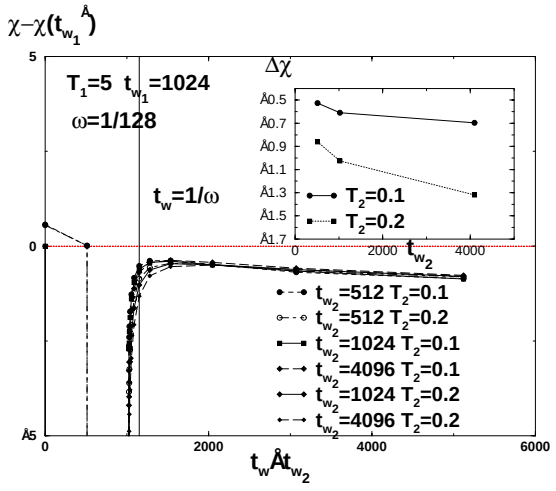

Figure 5.14. Memory anomaly in a negative temperature cycle at fixed ω. We plot the $\chi - \chi(t_{w_1}^-)$ at fixed $\omega = 1/128$ and $t_{w_1} = 1024$ for the temperature changes $T_1 = 5\ T_2 = 0.1, 0.2$ for different $t_{w2} = 512, 1024, 4096$. In the inset we plot $\Delta\chi$ as defined in (5.99) for the different t_{w2}.

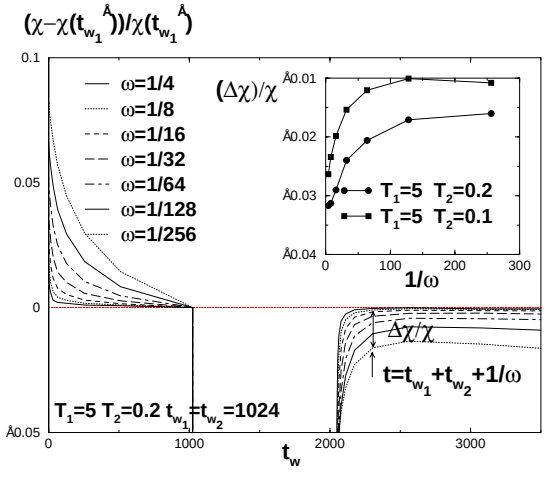

Figure 5.15. Memory anomaly in a negative temperature cycle at fixed ΔT. $\Delta\chi/\chi(t_{w_1}^-)$ for the cycle $T_1 = 5\, T_2 = 0.2$ with $t_{w_1} = t_{w_2} = 1024$ we plot $\Delta\chi/\chi(t_{w1}^-)$ for different frequencies, $\omega = 1/4....1/256$. In the inset we plot $\Delta\chi/\chi$ versus $1/\omega$ for this case and for the cycle $T_1 = 5\ T_2 = 0.1$ with the same parameters.

6. Discussion: excitations in dynamics

Let us summarise the main observations with respect to the chaos and rejuvenation problem. Temperature chaos reflects the decorrelation of free-energy landscapes at dif-

ferent temperatures. This situation is met if the system allows anomalously large gap-less excitations that are entropically favoured. These excitations must be of system size to ensure that they are far in phase space so that at different temperatures the statistics of different valleys describe equilibrium properties. Besides, entropy fluctuations must be large enough to overcome the (free-)energy cost. This is the situation met in the DPRM. In the droplet picture it is argued that these large excitations are the only ones relevant for the dynamics and thus the sole responsible for the striking dynamical effects such as rejuvenation.

All the same, in the analysis of the REEM we have seen that a large response to temperature changes can be observed in the absence of chaos when there is a transition characterised by a drastic change in the number of available states or so called entropy crisis. This is realised in the Sinai model at a dynamical level. At a given temperature, the system is able to equilibrate a region in phase space. On lowering the temperature, the system gets trapped in a smaller region of phase space because barriers become too large. Thus we say that the system is localised in fewer available states. At this point the dynamical evolution concerns only the local small excitations of the bigger valley explored at a higher temperature. In the Sinai model, the larger the temperature shift the more drastic this localisation and thus the larger the rejuvenation response. This response becomes infinite when this separation is infinitely sharp as in the REEM when there is a real thermodynamic transition in the infinite-volume limit. This is precisely the idea hidden in the hierarchical picture of which the Sinai model is the canonical example: at low temperatures the system probes a very small region in phase space so that it is not large droplets but small local excitations that bring about rejuvenation effects of the susceptibility in negative temperature shifts. Interestingly, from these observations it follows that not only large but small excitations are relevant for the dynamics. On the one hand, the ageing process would be linked with the existence of large scale droplets that are out-of-equilibrium, but, on the other hand, because at low T only small excitations are active the rejuvenation signal must be associated with them.

Chapter 6

CONCLUSIONS

A widespread idea in random systems with frustration is that the low-temperature physics is governed by the $T = 0$ fixed point [FH86]. So that any system can be depicted as a ground state plus a spectrum of excitations or droplets with low energy. In this thesis we have investigated several aspects of large-scale excitations in disordered systems in general. In spite of having developed the main part of the analysis in the spin glass framework, many of the ideas and results reported in this thesis are also applicable to other systems presenting a spectrum of excitations with no gap. Indeed, many dynamical phenomena observed in spin glasses are observed in other complex glassy systems, such as glasses or polymers, whose free-energy landscapes present many features in common. Precisely the complex structure of the free-energy landscape is what favours the existence of rare excitations that involve a finite fraction of the spin variables (or degrees of freedom) of the system and thus are well separated from the ground state in configuration space. In the many-valley description of the free-energy landscape, this amounts to say that there are several deep valleys contributing to the thermodynamics. From our analysis it follows that the existence of several well defined valleys in phase space (*i.e.* the existence of large-scale excitations) is what yields the typical behaviour of these systems at the equilibrium level. Nonetheless, small intra-valley excitations also contain information about the typical statics and dynamics. All the same, the main part of the analysis presented in this thesis has been carried out through scaling hypothesis valid, in principle, for large-size droplets.

The central part of this thesis turns around the study of the absolute lowest-lying excitations, this is to say, the excitations that are closest in energy to the ground state. This is a novel zero-temperature approach to study typical behaviour. As far as we can see, this expansion is valid for systems that allow large-scale excitations. Its validity for cases in which these excitations have a vanishing probability in the thermodynamic limit, (e.g. "replica symmetric phases" with $\theta > 0$) remains to be checked. In this approach we assume that the physics close to zero temperature of a system of size $V = L^d$ is

described by the ground state and the first excitation. This lowest-lying excitation is a cluster whose size (v) and gap (ϵ) are random variables. Regarding large-scale excitations, gap and volume distributions are characterised with the *lowest-droplet* exponents θ_l and λ_l respectively. The exponent θ_l describes the average energy gap $\overline{\epsilon} \sim L^{\theta_l}$, thus $\theta_l \leq 0$ and for finite-dimensional systems it is argued to be $-d$. The lowest-droplet exponent, λ_l, describes the probability of having a large lowest-lying excitation $\sim L^{-d\lambda_l}$, so that the average volume scales as $\overline{v} \sim L^{d(1-\lambda_l)}$, $\lambda_l > 0$. Remarkably, the knowledge of the statistics of these lowest-lying excitations is enough to determine the thermal exponent θ characterising typical excitations through the following relation $\theta = \theta_l + d\,\lambda_l$. The fact that the typical behaviour can be inferred from the analysis of non-typical excitations is due to the random nature of the spectrum of energy gaps. Based on numerical results, we have gathered the main features of this spectrum under the name of *uncorrelated energy-size scenario*: *i)* there are no correlations between energy gaps and *ii)* there are no correlations between gaps and excitation volumes. These two assumptions are very reasonable in systems with a rugged free-energy landscape where frustration induces the existence of a continuous band of energy levels within uncorrelated gaps. From here it follows that the knowledge of the thermal exponent is enough to determine the low-temperature behaviour of energy-related quantities such as the specific heat that vanishes as $c \sim T^{-d/\theta_l}$. Thereby it is linear provided $\theta_l = -d$, in agreement with the value obtained via extreme statistics arguments. Numerical investigations show that this thermal exponent has very large finite-size corrections so that the specific heat at low temperature is not linear in a finite system. On the other hand, quantities related to the overlap depend on both exponents (θ_l, λ_l) and, in particular, on the thermal exponent θ. Specifically, the weight at at $q = 0$, $P(q = 0)$, remains finite at finite temperature provided $\theta = 0$. In this case the volume distribution is equivalent to the $P(q)$ at low temperature as observed in a mean-field example, the SK model. Furthermore, the analysis of short-ranged models (EA in $d = 1, 2$) reveals that apart from fulfilling the uncorrelated energy-size assumptions, small size lowest-lying excitations yield the same contribution than large-scale excitations to any energy or overlap related quantity. This finding puts forward the idea that typical excitations that involve a large number of spins but that happen with finite probability at finite temperature are not necessarily single clusters but could consist of several clusters of small size.

In the first part of the thesis we have investigated the organisation of excitations in phase space through the measure of order parameter fluctuations in spin glass systems. In mean-field models, large excitations happen with finite probability in the thermodynamic limit. This means that there exist many degenerate free-energy valleys in phase space corresponding to different states. Thereby, the overlap between two of these states can take any value in the range $[0, 1]$, and thus is a random variable with non-vanishing fluctuations in the thermodynamic limit. Formally this is expressed as the breaking of replica symmetry at low temperatures and in the existence of sum rules between the joint probabilities of several overlaps. In this thesis we have studied mean-field models which OPF are finite, as well as short-ranged models for which the infinite-volume limit

behaviour is unknown. Nevertheless, in a finite system we expect OPF to be finite because there can exist large excitations with finite probability $\sim L^{-\theta}$. For this reason parameters measuring order parameter fluctuations, G and A, are a good numerical tool to study transitions into the spin glass phase of MF and short-ranged models, in contrast to other parameters such as the Binder cumulant which are only sensible to the breaking of time-reversal symmetry. In mean-field models, with or without TRS, these parameters work very well even for very small systems. Besides, the behaviour of these parameters, as well as the connected quantities can be computed exactly. In RS phases where $\theta > 0$, G and A are ratios of quantities which vanish in the thermodynamic limit, but that for finite systems have contributions coming from rare anomalously large excitations. This is the reason why very high precision statistics is needed to compute OPF parameters. Thus, in systems where TRS is broken at the transition these parameters do worse than the Binder cumulant at locating the exact transition as observed in the EA model in 3d.

Notwithstanding this, these parameters are very useful to characterise the low-temperature phase. A remains finite in the large size limit provided there is RSB below T_c, whereas G takes a finite value even when OPF vanish. In mean-field models that display RSB, G is equal to $1/3$ in the frozen phase because the sum rules hold strictly hold at any temperature. In RS phases G remains also finite, despite being the ratio of two quantities that vanish in the thermodynamic limit. The numerical results of all the models studied support the conjecture that indeed $G = 1/3$ below T_c in the thermodynamic limit in any spin glass model. This suggests that finite-size contributions to OPF in models with $\theta > 0$ verify the sum rules. On these grounds one can assume that, at least in finite systems, the organisation of valleys is similar to that of mean-field models. In fact, Guerra proved that these sum rules hold in systems with disorder that are stable with respect to a random perturbation of mean-field type (this is the property of stochastic stability) [Gue96]. However, the systems to which this treatment applies has remained rather obscure. Furthermore, all parameters measuring OPF are found to take universal values at $T = 0$ for any finite volume provided the ground state is unique with a spectrum of gap-less excitations. This general result has been derived in the framework of the lowest-excitation expansion, from which one learns the following conclusions: that the sum rules of the probability distribution of the overlap hold in any system at least at order T and that at low temperature A vanishes as $\sim TL^{-\theta}$ with θ being the exponent. This last assertion has been confirmed in short-ranged models in 1 and 2 dimensions. Since there is a critical point at $T = 0$, the droplet exponent is related to the correlation length exponent $\theta = -1/\nu$ and, thus, can be obtained also from the scaling behaviour of adimensional parameters such as the Binder ratio, producing the same numerical values for θ.

In the last part of the thesis, we have analysed the so called chaos problem, or in other words the dependence of the free-energy landscape in temperature. We say that a system is chaotic if introducing a perturbation δ causes a change of the equilibrium state or equivalently leads to the decorrelation of the free-energy landscape. Here we have investigated energy landscapes of different systems that allow gap-less large excitations to

find out under what conditions the free-energy landscape is chaotic. The phenomenology of chaos is the same as that of phase transitions, with δ playing the role of $\epsilon = (T-T_c)/T_c$, thus the limits $L \to \infty$ and $\delta \to 0$ do not commute. In analogy to the correlation length, one can define an overlap length $L_c \sim \delta^{-\zeta}$, ζ being the so called chaos exponent, that separates the weak and large perturbation regimes and diverges when $\delta \to 0$ because the equilibrium configuration remains unchanged. Remarkably, the onset of chaos acquires in physical space the particular meaning of spontaneously breaking replica symmetry, as well as in the transitions of mean-field spin-glass models. Within this context, the introduction of a perturbation amounts to a repulsive term in the Hamiltonian which is polynomial in n, the replica index. If we keep the replica index finite, we observe that there is a crossing of levels corresponding to RS and RSB solutions. This crossing of levels is identified with the crossover from weak to strong perturbation regimes from which one can infer the crossover length scale. In fact, the order of the perturbation in the replica index determines the universality class of each perturbation because it is directly related to the chaos exponent describing the overlap length.

The chaoticity against bond or magnetic perturbations has been extensively reported in various systems where large excitations are present [Rit94, NN97]. Here, the main interest has been to study temperature chaos. The analysis of response and correlation functions tells us that decorrelation is possible if entropy fluctuations are large enough to compensate the energy cost. In the DPRM problem this is possible because energy and entropy fluctuations cancel to yield much smaller free-energy fluctuations. In fact, we have observed that, regarding exponents, temperature and bond chaos belong to the same universality class. In spin glasses it is not clear whether this scenario holds. Recent results on the SK model show the temperature perturbation has the same critical exponents as the bond perturbation but with a much smaller amplitude [Rit94, CR02a]. However, it could well happen that temperature chaos is a less effective perturbation because it has a bigger chaos exponent.

We have also investigated a model closely related to the DPRM, the Sinai model. Both systems have no transition and thus are always in the glassy phase. However, the physics of the Sinai model is absolutely governed by the ground state. Entropy in this model does not play any role, so that excitations have an enormous free-energy cost and cannot be favoured by the temperature perturbation. Still, the study of the low-T phase of the REEM, a mean-field model without chaos, reveals that the existence of a real thermodynamic transition driven by an entropy collapse can produce a large response to temperature changes. This finding provides a new mechanism to explain rejuvenation, and numerical investigations on related models have produced results similar to experimental observations [Kaw01, SVDV02]. This same situation is met dynamically in the Sinai model, because length scales are exponentially separated by temperature. However, this separation is not as sharp as in the REEM because there is no real phase transition. For this reason, the rejuvenation and memory effects observed are a smeared out version of those that arise from drastic separation between length scales. Nevertheless, the interesting fact is that as this model is strictly self-similar, the details probed at low temperature are

independent of the specific valley occupied before the quench. The outcome is that these local excitations do bring about strong rejuvenation signals upon negative temperature shifts. Thus there is no need of chaos, *i.e.* of large excitations, to produce rejuvenation signals dynamically.

In summary, the study of excitations reveals that the random nature of disordered systems is reflected in the spectrum of lowest excitations. This is the reason why studying first excitations (that are not typical) one can describe the equilibrium behaviour at finite temperatures. Remarkably, in short ranged systems both small (intra-valley) and large (off-valley) lowest excitations yield the same contributions, suggesting that both types of excitations are relevant. From the investigation of order-parameter fluctuations the picture that one gets from the lowest-lying excitations is that at least for finite system sizes, excitations are organised following a mean-field like structure. The study of the chaos problem reveals that only if large-size excitations are entropically enhanced there can be decorrelation effects in the free-energy landscape. Nonetheless, these large-scale phenomena do not necessarily account for dynamical signals at low temperature because these length scales are presumably frozen, so that the activation of small local excitations relevant at low temperatures is the responsible for the *restart* of the ageing process.

Open problems and future research

At the end of a thesis one expects to have answered some of the questions posed at the beginning. Nevertheless, there are still several aspects that would deserve further investigation and, besides, many different problems that emerge from the ideas developed in this work. There are several points that I would like to highlight.

Regarding the study of OPF it is evident that it remains an open problem the proof of the conjecture that parameter $G = 1/3$ below T_c in the thermodynamic limit. The search of an answer to this problem can be very instructive since it implies understanding the organisation of lowest-lying excitations in any spin-glass model. Certainly, the investigations from low-temperature expansions are very appealing, but the inclusion of higher order excitations is not trivial. In the same context, I think that it could be interesting to exploit the connection between p-spin models and structural glasses. One could define parameters equivalent to G and A where the averages over the samples are substituted by averages over different configurations. In my opinion this could be a different point of view to study the liquid-glass transition that might yield useful information. In this same direction, the analysis of the connected quantities G_c, A_c and B_c would be interesting because we have seen that they only depend on temperature through the RSB parameter m which is related to the FDT violation factor in glasses.

As far as low-temperature expansions are concerned one of the most complex problems is that of going to higher orders, since it implies understanding how are the correlations between excitation volumes of excitations occupying different levels in the spectrum. However, as far as I can see, this question cannot be answered without numerical investigations of larger systems than the ones studied here, at least for the 2d EA model. In this direction, the analysis of the 3d EA model, even for modest sizes, would be also

very instructive. Still, there are also several extensions of the lowest-excitation approach presented here that could be interesting, such as the analysis of the properties of the surface of first excitations through investigations of the link overlap, as well as the study of the effects of a magnetic field in the volume and gap distributions. As far as mean-field models are concerned, the extension of the analysis of the SK model to $p-$spin models with $p > 2$ is very appealing. In particular, the study of the dependence of Θ_l with p. We have seen that for $p = 2$, $\Theta_l = -.5$ whereas in the limit $p \to \infty$ (or the REM), we know from extreme value statistics that $\Theta_l = 0$ [BM97]. Thus, it would be interesting to see what is the shape of this $\Theta_l(p)$ and what are the effects on the specific heat at low temperatures, which according to the results reported here should not be linear in T. Notably, this problem can be studied numerically and analytically, since the possibility of computing the distribution of local-fields through TAP equations offers a good starting point for analytical treatment of this problem. Besides, it remains totally unexplored the dynamical counterpart of this analysis. Or in other words, how the distribution of excitations and energy costs corresponding to large-scale excitations is realised dynamically in large samples.

In the chaos problem there are two questions that attire my attention. The first one is to discern between chaos induced by critical fluctuations and true chaos in the frozen phase. For instance, one could study a model such as the DP in 1+2 dimensions, which has a transition at finite temperature but is believed to have the same low-temperature properties as the DP in 1+1 dimensions studied in this thesis. The interest would be to see if the response against external perturbations changes or not at the critical temperature. Following this same direction, it would be interesting to see compare the chaotic properties of systems with different types of transitions. Of course, the link between this analysis and the problem of rejuvenation is straightforward, and the interest is to see what mechanisms lead to rejuvenation and which do not by performing numerical simulations of temperature cycling experiments around the critical region. Thus, in a systems like the DP in 1+2 dimensions, the analysis of temperature cycling experiments is interesting for two reasons, *i)* to study differences in the ageing process in different temperature regions (frozen and critical) and *ii)* to study what is the dynamical phenomenology that characterises the existence of a weak perturbation regime in comparison to that observed in non-chaotic systems such as the multi-layer REM or the Sinai model.